Tarach, KA.; Martínez-Triguero, J.; Rey Garcia, F.; Góra-Marek, K. (2016). Hydrothermal stability and catalytic performance of desilicated highly siliceous zeolites ZSM-5. Journal of Catalysis. 339:256-259. doi:10.1016/j.jcat.2016.04.023.

Hydrothermal stability and catalytic performance of desilicated highly siliceous zeolites ZSM-5

Karolina A. Tarach[a], Joaquin Martinez-Triguero[b*], Fernando Rey[b] and Kinga Góra-Marek[a**]

[a] Faculty of Chemistry, Jagiellonian University in Kraków, 3 Ingardena St., 30-060 Kraków, Poland

[b] Instituto de Tecnología Química, Universidad Politécnica de Valencia, Camino de Vera s.n., 46022 Valencia, Spain

Corresponding authors:

** Faculty of Chemistry, Jagiellonian University in Kraków, 3 Ingardena St., 30-060 Kraków, Poland, phone +48 (12) 663-20-81, fax. +48 (12) 634-05-15

email: kinga.goramarek@gmail.com

* Instituto de Tecnología Química, Universitat Politècnica de València-Consejo Superior de Investigaciones Científicas, Avenida de los Naranjos s/n, 46022 Valencia, Spainemail: jomarti@itq.upv.es

ABSTRACT

Highly siliceous zeolites, namely MFI type have attracted the great attention due to their higher hydrothermal stability, higher selectivity to organic compounds, and often better catalytic properties in comparison to Al-rich zeolites. The native zeolite (Si/Al = 164) and its desilicated analogues were deeply characterized with regard to their structural and textural properties by X-ray diffraction, low temperature adsorption of nitrogen and solid-state ^{27}Al MAS NMR. Their acidic properties were evaluated in quantitative IR studies. Finally, the catalytic performance of desilicated zeolites ZSM-5 was evaluated in the cracking of *n*-decane, 1,3,5-tri-iso-propylbenzene and vacuum gas oil. In this article, it is shown that high silica zeolites prepared by NaOH and NaOH&TBAOH leaching presented good hydrothermal stability with only slightly lower resistance when comparing to native steamed zeolite. The mesoporosity was preserved after the steaming treatment. The influence of the generated mesoporosity on the higher activity was evidenced in both 1,3,5-tri-isopropylbenzene and diesel oil cracking of steamed hierarchical zeolites. In spite of their lowered acidity, the mesopores system benefited the diffusion of the bulky molecule and finally provided higher activity of hierarchical zeolites.

Keywords: hierarchical zeolites; ZSM-5; desilication; TIPB; *n*-decane; cracking; FCC

1 INTRODUCTION

Major difficulties resulting in deactivation of the catalysts have been reported when using aluminium-rich zeolites, namely the coke formation and dealumination at high temperature in a water vapour presence [1]. Thus, the great attention has been paid to synthesis of highly siliceous zeolites characterized by higher hydrothermal stability and often better catalytic properties in comparison to Al-rich zeolites [2-4].

Catalytic applicability of zeolites, being efficient catalysts for the rearrangements of small molecules, is strongly reduced for the bulky ones due to the diffusional limitations. This diffusional constrains can be decreased by a generation of an intracrystalline mesopore system of the controlled pore size distribution. Different routes have been designed to induce the additional mesoporosity in zeolite crystals. Porous carbon or carbon nanotubes as well as mesoscale cationic polymers are commonly used during templating methods [5-7]. Further modifications include synthesis of nanosized zeolite crystals, zeolitization of mesoporous materials and recrystallization [8]. Among these methods, desilication, a process of the controlled alkaline leaching of the silicon atoms from the zeolite's framework, has been described as the one of the most effective approaches for the hierarchical zeolites tailoring [9-12]. Apart from the versatility and simplicity, the main achievement of desilication is related to a number of parameters that may be optimized to obtain hierarchical zeolites. The number of silicon atoms that could be removed with crystallinity preservation is governed by Si/Al ratio and the framework topology as well as by the type and concentration of desilicating agent used. The main part of desilication studies has been devoted to zeolites of medium Si/Al ratio (25-50) where the presence of Al atoms influences the extent of the Si removal [13]. Desilication of highly siliceous zeolites have been less frequent approach due to the difficulties in the efficient generation of extra mesoporosity. Nevertheless, desilication of silicalite-1 with tetrapropylammonium cation (TPA^+) as a pore directing agent (PDA) and in the presence of aluminium nitrate has been reported by Verboekend et al. [14]. It has been proven for the first time that framework aluminium is not a prerequisite for the introduction of intracrystalline mesoporosity by desilication [14]. The role of the affinity of zeolite surface to PDA and their efficiency in mesopores formation has been also discussed [15, 16]. Finally, the precisely tailored porosity affecting the acidity of mesostructured zeolites is reflected in the variety of the fabricated acidic sites and their accessibility. Among methods offering the comprehensive acidic properties depiction, IR spectroscopy is one of the most powerful tool. When probe molecules are employed, the number and strength as well as the location of acid sites in zeolites can be achieved [17-20].

Fluid catalytic Cracking (FCC) is the second largest propylene production source producing 30 % of the world propylene demand. Owing to the increase in the demand for propylene, FCC has become an

important backup in improving the propylene production: new catalyst preparations, their modification, and additives are some of the options. Among them, easiest and cheapest method to improve propylene yield is the use of zeolite ZSM-5 additives in FCC. The ability of ZSM-5 to increase the light olefins yield from the FCC is attributed to the size and shape of its channels. The small pores of zeolite ZSM-5 allow the diffusion and cracking of low octane, linear hydrocarbons from the gasoline into LPG range olefins. Finally, the gasoline becomes enriched in aromatic compound and the octane value increases. Otherwise, the application of hierarchical zeolite ZSM-5 for gasoil cracking has been recently studied [21, 22]. The generated mesoporosity increases the yield of middle distillates while lowering significantly the capability to catalyst cocking and increases the yield of propylene due to the presence of more accessible catalytic surface with shorter paths which limit secondary and hence, hydrogen transfer reactions

The aim of this work was to investigate the stability of hierarchical highly siliceous zeolites ZSM-5 (Si/Al=164). Therefore we carried out the detailed studies of the textural and acid properties of the hierarchical zeolites both after being tested in the cracking reactions and steamed in the conditions typical of the FCC catalyst regeneration. The influence of steaming conditions on the acid properties of desilicated zeolites was followed by NMR and IR spectroscopies. The ^{27}Al MAS NMR measurements delivered information on the status of Al atoms in both native and desilicated zeolites as well as on the changes of this status upon the steaming process. The concentration of Brønsted and Lewis acid sites was measured in quantitative IR studies of pyridine sorption, while their strength were determined in pyridine thermodesorption experiments and low temperature carbon monoxide sorption. Catalytic properties of desilicated zeolites, both non-steamed and steamed, were followed in the cracking of n-decane, 1,3,5-tri-isopropylbenzene and vacuum gasoil, and then were correlated with acidity of active sites. Linear *n*-decane molecules are allowed to easily penetrate the channels of ZSM-5 zeolite therefore, catalytic activity in *n*-decane cracking is dependent on the accessibility of the protonic sites in minor extend. On the other hand, the accessibility of protonic sites was determined when using the cracking of 1,3,5-tri-isopropylbenzene as a test reaction.

2 EXPERIMENTAL

2.1 Catalyst preparation

Desilication of the native ZSM-5 zeolite (Si/Al = 164, Zeolyst International, CBV 28014) was carried out in the solution of 0.2 M NaOH and in the mixture of 0.2 M NaOH and 0.2 M TBAOH (tetrabutylammonium hydroxide) at 65 °C for half an hour. For the 100 ml mixture of NaOH&TBAOH the 40 ml of 0.2 M TBAOH and 60 ml of 0.2 M NaOH was taken. The 100 ml of solution was added to 3.0 g of zeolite. After desilication the suspension was cooled down in ice-bath and filtered. The hierarchically structured zeolites were washed with water until neutral pH. Next a fourfold ion-exchange with 0.5 M NH_4NO_3 was performed at 60 °C for 1 h. Finally, the zeolites were again filtrated, washed and dried at room temperature. The resulting **desilicated** materials were denoted hereafter as **D**_NaOH/ZSM-5 and **D**_NaOH&TBAOH/ZSM-5. These materials subjected the catalytic vacuum gas oil cracking **reactions** were denoted as **R**/ZSM-5, **R**&D_NaOH/ZSM-5 and **R**&D_NaOH&TBAOH/ZSM-5 (Table 1).

Steaming of native and hierarchical ZSM-5 zeolites was performed in 650 °C and 700 °C under continuous liquid water injection with 1.8 cm^3min^{-1} flow speed for 3 hours. The catalysts were preheated from RT to steaming temperature during 2 hours. The resulting **steamed** materials were denoted hereafter as **S**/ZSM-5, **S**&D_NaOH/ZSM-5 and **S**&D_NaOH&TBAOH/ZSM-5 (Table 1).

The scheme representing of the sample modifications is presented in Figure 1.

2.2 Characterization methods

2.2.1 Structural and textural parameters

Si and Al concentrations in the parent and desilicated zeolites were determined by the ICP OES method with an Optima 2100DV (PerkinElmer) spectrometer.

The powder X-ray diffraction (XRD) measurements were carried out using a PANalytical Cubix diffractometer, with CuK_α radiation, λ=1.5418 Å and a graphite monochromator in the 2θ angle range of 2-40°. X-ray powder patterns were used for structural identification of the relative crystallinity value (%Cryst) for all the zeolites. The determination of the relative crystallinity value was based on the intensity of the characteristic peaks in the range between 22.5° to 25.0°.

The N_2 sorption processes at -196 °C were studied on an ASAP 2420 Micromeritics after activation in vacuum at 400 °C for 12 h. Surface Area (S_{BET}) and micropore volume (V_{micro}) were determined by applying the BET and *t*-plot methods, respectively. Pore size distribution and volume of mesopores (V_{meso}) were obtained by applying the BJH model to the adsorption branch of the isotherm. The

mesopore surface area (S_{meso}) was calculated in the range between 2 and 30 nm with BJH model and it denotes external surface area.

Transmission electron microscopy was carried out with using a Philips CM-10 microscope operating at 100 kV. The samples under investigation were initially ultrasonically dispersed in 2-propanol and then transferred to carbon coated copper grids.

2.2.2 XPS analysis

The X-ray photoelectron spectra (XPS) were measured with a Prevac photoelectron spectrometer equipped with a hemispherical VG SCIENTA R3000 analyser. The photoelectron spectra were measured using a monochromatized aluminium AlKα source (E=1486.6 eV) and a low energy electron flood gun (FS40A-PS) to compensate the charge on the surface of nonconductive samples. The base pressure in the analysis chamber during the measurements was $5 \cdot 10^{-9}$ mbar. Spectra were recorded with constant pass energy of 100 eV for the survey and for high resolution spectra. The binding energies were referenced to the Si 2p core level (103.0 eV). The composition and chemical surrounding of the sample surface were investigated on the basis of the areas and binding energies of Al 2p, Si 2p and O 1s photoelectron peaks. The fitting of high resolution spectra was provided through the CasaXPS software.

2.2.3 MAS NMR studies

The solid state MAS NMR spectra were acquired on a Bruker AV400 spectrometer. Prior to ^{27}Al MAS NMR measurements the samples were kept in 75% relative humidity for 48 hours. The frequency scales in ppm were referenced to 1 M solution of $Al^{3+}(H_2O)_6$. The ^{27}Al MAS NMR were recorded at 79.46 MHz, 60º pulse length and 60 s recycle delay. Spectra were normalized to the same mass of sample.

2.2.4 IR studies

Prior to the FTIR study all samples were pressed into the form of self-supporting wafers (ca. 5 mg/cm^2) and pre-treated in situ in homemade quartz IR cell at 550 ^oC under vacuum conditions for 1 hour. The IR spectra were recorded with a Bruker Tensor 27 spectrometer equipped with a MCT detector. The spectral resolution was 2 cm^{-1}.

The concentration of Brønsted and Lewis acid sites determined in quantitative IR studies of pyridine adsorption, in line with the procedure given in ref. [23]. The values of 0.10 cm^2/μmol and 0.06 cm^2/μmol were applied for the 1450 cm^{-1} band of pyridine coordinatively bonded to Lewis sites (PyL) and for the 1545 cm^{-1} band of pyridinium ion (PyH^+), respectively.

The acid strength determined in pyridine thermodesorption and carbon monoxide adsorption studies. In the pyridine thermodesorption experiments, the conservation of the 1540 cm^{-1} (Brønsted sites) band under the desorption procedure at 500 °C was taken as a measure of the acid strength of the acid sites. The sorption of CO as probe molecule was performed at -100 °C. The downshift of IR band of the acidic hydroxyls (3200–3800 cm^{-1}) due to their interaction with adsorbed CO molecules was taken as a measure of the acid strength.

2.3 Catalytic tests

The cracking experiments were performed in a MAT (Micro Activity Test) unit described previously [24, 25]. The pellets of zeolites were crushed and sieved; fraction of the 0.59–0.84 mm was taken for cracking reactions. For each catalyst, catalytic experiments were carried out, preserving the amount of catalyst (cat) constant and varying feeds amounts (oil). Four cracking reactions with different cat-to-oil ratios of 1,3,5-tri-iso-propylbenzene (TIPB) were performed, while for n-decane and gas oil cracking five experiments were carried out. Detailed description of the catalytic tests is presented in Table 2. The evaluation of hierarchical zeolites ZSM-5 in cracking reactions was performed with use of vacuum gas oil as the feed of the composition listed in the Table 3.

Gases were analysed by Gas Chromathography in a Rapid Refinery Gas Analyser from Bruker (450-GC) and simulated distillation of liquids in a Bruker SIMDIS.

Kinetic rate constants (k) were calculated by fitting the conversions (X) to a first-order kinetic equation for a plug flow reactor (1) for *n*-decane and TIPB or to a second order kinetic equation for a plug flow reactor (2) for gas oil, assuming that the deactivation is enclosed in the kinetic constant and taking into account the volumetric expansion factor (3),

$$k = -(\text{cat oil}^{-1}\text{TOS})^{-1}[\varepsilon X + (1+\varepsilon)\ln(1-X)] \quad (1)$$

$$k = -(\text{cat oil}^{-1}\text{TOS})^{-1}[X/(1-X)] \quad (2)$$

$$\varepsilon = (\Sigma\text{molar selectivities of products}) - 1 \quad (3)$$

These rate constants were used to compare the activities of the catalysts with their textural and acidic properties.

3 RESULTS AND DISSCUSION

3.1 Structural and textural parameters

The values of Si/Al ratio for the parent and desilicated zeolites were listed in the Table 4. Zeolite NaOH&TBAOH-treated was less extensively desilicated than that leached with NaOH only. This phenomenon, explained by protection of zeolite surface by TBA^+ cations against OH^- ions attack, is widely described in the literature [26, 27]. Analysis of the XRD patterns (Fig. 2) confirmed that desilication with both NaOH and NaOH&TBAOH mixture did not disturb the crystallinity of resulting hierarchical materials (Table 4), the zeolite structure was maintained (crystallinity decreased from 100% to 88%). The values of both the mesopore surface and volume are presented in Table 4. The pore size distributions determined by using BJH model was presented in Fig. 3. The treatment of zeolite with NaOH (D_NaOH/ZSM-5 sample) resulted in the formation of mesopores of various diameters; however a broad maximum in diameter distribution at ca. 20 nm can be seen. Both surface and volume of mesopores increased upon desilication. The addition of TBAOH to NaOH (D_NaOH&TBAOH/ZSM-5) resulted in a distinct modification of mesopore size; the pore size distribution became narrower and, consequently, the maximum in diameter distribution is centred on 10 nm. TEM micrographs (Fig. 4) verified additionally the generation of the uniform system of mesopores in the crystals of NaOH&TBAOH-treated zeolite, D_NaOH&TBAOH/ZSM-5. The sample treated with NaOH&TBAOH presents a wide hysteresis loop in the nitrogen isotherm with a closure point around 0.4 value of p/p_0. This wide hysteresis has been related to the presence of constricted mesopores in which nitrogen only can access through the micropores and not directly from the surface of the crystals [28, 29]. Independently from temperature, the steaming of both native S/ZSM-5 and desilicated zeolites, S&D_NaOH/ZSM-5 and S&D_NaOH&TBAOH/ZSM-5, did not affect the hierarchical structure; mesoporosity was preserved during steaming process. Additionally, the volume of micropores almost did not change even after steaming in relatively severe conditions (Table 4).

The ^{27}Al MAS NMR measurements as the most powerful tools to monitor the status of Al atoms in zeolites [27, 30, 31] allowed us to follow the changes of this status upon post-synthesis modifications e.g. steaming process. The ^{27}Al MAS NMR spectra of native zeolite ZSM-5 and the same zeolite after catalytic reaction (R/ZSM-5) as well as contacted with steam at 650°C and 700 °C (S650/ZSM-5 and S700/ZSM-5)) and then subsequently used in the reaction are presented in Figure 5. The spectrum of the non-steamed zeolite consists of, as the only moiety, an intense signal at 51 ppm assigned to tetrahedral Al(IV) at the zeolite framework.

For the S650/ZSM-5 sample steamed at 650 °C and subsequently tested in cracking a weak signal at 0 ppm typical of extraframework octahedral aluminum species Al(VI) appears. At the same time, the

drop of the Al(IV) signal and its broadening is observed. These findings indicate that steaming resulted not only in the transformation of tetrahedral Al(IV) species into octahedral Al(VI) ones but it also significantly affected the geometry of framework, thus the distorted tetrahedral Al(IV) species were created. In the case of the native zeolite S700/ZSM-5 neither higher steaming temperature (700 ^{o}C) nor subsequent using in the catalytic reaction affected the status of aluminium more. Similarly, the scrutiny of the ^{27}Al MAS NMR spectra for desilicated zeolites steamed at 650 ^{o}C and tested in cracking reactions provides the same results, nevertheless, the extend of the Al(IV) removal from framework positions, defined by the drop of the Al(IV) signal, is much more noticeable. Higher temperature of steaming (700 ^{o}C) further affected the framework composition because, in the contrast to native zeolite, the distinct amount of Al(IV) were removed to octahedral positions. All these results provide an evidence for lower hydrothermal stability of aluminium species in hierarchical zeolites. It should be noted that the signal typical of Al(VI) species is hardly detected in the ^{27}Al MAS NMR spectra and its intensity does not match the drop of the Al(IV) signal observed for steamed zeolites. This phenomenon, assigned to the presence of strongly disturbed octahedral aluminium species in steamed samples, is widely discussed in the literature [32-35].

3.2 XPS analysis of studied catalysts

The analysis of chemical composition of surface of desilicated zeolites was performed with use of the XPS method by following the changes in relative concentration of silicon and aluminium by the Al 2p and Si 2p electron levels (Table 6). The obtained values of Si/Al ratios on the surface and in the bulk for parent and desilicated zeolites pointed to accumulation of Al species on external surface of grains caused by desilication process. Significant amount of extraframework aluminium species, probably acting as the Lewis acid centers, located on external surface of zeolite grains for sample desilicated with use of NaOH, can, despite enhanced mesopore surface area, negatively influence the catalytic performance in cracking of TIPB molecules (See Section 3.4.2).

3.3 Concentration and strength of acid sites

At the experimental reaction conditions and in the presence of water produced during the regeneration of the catalyst at high temperature, the activity of the zeolitic component of the catalyst is reduced due to the irreversible dealumination that decreases its Brønsted acidity [1]. Therefore, the impact of the temperature of steaming (650 and 700 ^{o}C) on the acidic properties of the zeolite was examined with the use of quantitative studies of pyridine adsorption.

The concentration of both Brønsted and Lewis acid sites was determined with pyridine in quantitative IR experiments [23], and then compared to the concentration of Al from chemical analysis (Table 5). In native zeolite ZSM-5 the concentration of protonic sites was found to be very close to the

concentration of Al from chemical analysis (85 and 94 µmol/g). Negligibly low concentration of Lewis acid sites (7 µmol/g) was detected proving that nearly all Al atoms were in framework positions and formed acidic Si-OH-Al groups. Desilication with both NaOH and NaOH&TBAOH led to the lowering of the concentration of protonic sites and the appearance of the significant amounts of Lewis acid sites in zeolites D_NaOH/ZSM-5 and D_NaOH&TBAOH/ZSM-5. The concentration of protonic sites was found to be 20–40% lower than concentration of Al. Information on the accessibility of acid sites located on the surface of mesopores as well as in the pore mouths was derived from quantitative IR studies of pivalonitrile adsorption [19]. It can be clearly seen that the desilication process performed in the presence of NaOH&TBAOH mixture assured the highest accessibility of acid sites, independently from their type (Table 5). Effectively developed mesopore system with enhanced amount of pore mouths on external surface is responsible for the high accessibility of Brønsted acid sites. On the other hand, the results of quantitative IR studies of pyridine and pivalonitrile sorption can suggest that the steaming process leads to the formation of Lewis acid sites located solely inside of micropores.

The analysis of (a) the position of the band of freely oscillating Si(OH)Al groups (Fig. 6), (b) the $\Delta\nu_{OH\ldots CO}$ values of hydroxyls engaged in hydrogen bonding with CO and (c) the A_{500}/A_{170} values from pyridine thermodesorption evidenced the decrease of the acid strength of protonic sites for desilicated materials (Tables 7). The same effect has been previously reported for alkaline leached ZSM-5 zeolite of Si/Al = 31.6 [27]. The decrease of the acid strength can result from extraction of Al atoms forming the most acidic Si(OH)Al groups which are the less stable in zeolite framework, and therefore are supposed to be removed in the first order. After the cracking reactions the native zeolite ZSM-5 is found to keep a full acidity, while for hierarchical materials a small decrease in the concentration of acid Brønsted centers (from 101 to 95 $\mu molg^{-1}$ for NaOH-treated zeolite and from 95 to 72 $\mu molg^{-1}$ for NaOH&TBAOH-treated material) is observed (Fig. 7). Simultaneously, an increase of the concentration of Lewis acid centers (from 30 to 40 $\mu molg^{-1}$ for NaOH-leached and from 33 to 56 $\mu molg^{-1}$ for NaOH&TBAOH-leached sample) is evidenced (Fig. 7). The largest decline in the Brønsted acid sites concentration is observed for zeolite D_NaOH/ZSM-5, and at the same time, a large increase in the concentration of the Lewis acid sites is confirmed. With the increase of steaming temperature (from 650 to 700 °C) this effect is more pronounced: a half of Brønsted acid sites in the native ZSM-5 turned out to be not resistant for the hydrothermal treatment and they were transformed into extraframework Lewis sites. The less stable structure of desilicated zeolites more facilitated such transformation and consequently the concentration of Lewis sites was significantly higher for alkaline leached zeolites. The highest contribution of extraframework material was evidenced for steamed NaOH treated zeolite S650&D_NaOH/ZSM-5 pointing to its lowest hydrothermal stability. Summing up, pyridine sorption (Fig. 7) revealed the drop of the concentration of Brønsted sites accompanied by

an increase of the Lewis sites concentration. The ^{27}Al MAS NMR results also evidenced lower stability of tetrahedral aluminium Al(IV) in desilicated zeolites in comparison to native one, however, the drop of the intensity of the Al(IV) signal did not correspond to proportional increase of the intensity of the Al(VI) signal (Chapter. 4.2). It suggests that easily detectable in IR studies extraframework aluminium atoms, are highly disturbed thus not visible by ^{27}Al MAS NMR.

3.4 Catalytic tests

The nearly the same values of the conversion obtained for first and last experiment with the same amount of feed clearly confirm the textural and acidic properties maintenance.

3.4.1 Cracking of *n*-decane: the impact of microporous and mesoporous acidity

Catalytic properties of desilicated zeolites are influenced both by acidity of sites as well as their accessibility to reagents' molecules. For high silica zeolites with a low amount of protonic sites, the cracking of linear paraffin undergoes according to protolytic mechanism thought to occur via carbonium ions [36, 37]. Linear *n*-decane molecules are allowed to easily penetrate the channels of ZSM-5 zeolite. Thus, catalytic activity in *n*-decane cracking is principally ruled by intrinsic acidity of Brønsted sites. Consequently, the density and the strength of protonic sites are decisive factors for this reaction.

The catalytic properties of zeolite were evaluated on the basis of the conversion values and the K_{C10} value of reaction rate constants (Table 8). The *n*-decane conversion for D_NaOH/ZSM-5 and D_NaOH&TBAOH/ZSM-5 desilicated materials is only slightly lowered when comparing to native ZSM-5. The same, the parent ZSM-5 revealed the highest value of reaction rate constants for *n*-decane (k_{n-C10}) while desilicated zeolites are characterized by lower k_{C10} values. However, the advantage of the D_NaOH&TBAOH/ZSM-5 material over D_NaOH/ZSM-5 is clearly seen. This tendency is in line with the acid strength of protonic sites in non-steamed samples driven from both pyridine sorption and low temperature CO adsorption (Table 7). The decrease of both conversion and reaction rate k_{n-C10} matches with the acid strength of Brønsted centers: the native ZSM-5 possess the strongest acid sites and thus provides the highest catalytic activity, while the D_NaOH/ZSM-5 material with the sites of the smallest strength gives the lowest activity. The small differences in the values of the concentration of protonic sites among studied materials, obtained from quantitative experiments of pyridine sorption, seem not to have a significant impact on the k_{C10} value.

Independently from temperature of steaming, both native S/ZSM-5 and desilicated materials S&D_NaOH/ZSM-5 and S&D_NaOH&TBAOH/ZSM-5 demonstrate a significant drop in the value of the catalytic reaction rate constants (k) for the cracking of *n*-decane (Table 8). The smallest decline is

observed for native material. A little more stable, at the lower temperature of steaming (650 °C) appears to be a NaOH&TBAOH - treated zeolite. It should be underlined that only the S/ZSM-5 kept the level of conversion exceeding values typical of thermal cracking (Fig. 8). In turn, steaming at 700 °C did not lead to significant changes in the catalytic activity of zeolite S&D_NaOH/ZSM-5, however, again the activity of zeolite leached with the mixture of NaOH&TBAOH (i.e. S&D_NaOH&TBAOH/ZSM-5) was significantly lowered (Fig. 7, Table 8).

The selectivity of *n*-decane cracking reaction to liquids and gases for desilicated zeolites D_NaOH/ZSM-5 and D_NaOH&TBAOH/ZSM-5 remained unchanged when comparing to native one. The fresh and steamed at 650 °C desilicated with NaOH&TBAOH samples (D_NaOH&TBAOH; S650&D_NaOH&TBAOH/ZSM-5) represent highest olefinicity in the C_3 and C_4 fraction (Fig. 8A and B, $C_{3=}/C_3$, $C_{4=}/C_4$, $iC_{4=}/iC_4$ ratios) and produces less coke at the same time. On the other hand, the zeolite D_NaOH/ZSM-5, independently from thermal treatment (fresh, steamed at 650 °C or 700 °C), exhibited a slightly higher tendency for hydrogen-transfer reactions (HT), which is reflected as a decrease of $C_{3=}/C_3$, $C_{4=}/C_4$, $iC_{4=}/iC_4$ ratios. An important effect observed for zeolite with secondary system of mesopores is lower ability in coke formation during cracking reactions which resulted in a slower deactivation of the catalysts. This finding indicates that diffusional restrictions for secondary products were avoided and the transport of reagents within zeolite grains was improved. The steaming process at 700 °C led to the reduction of Brønsted characteristic while the Lewis acidity increased, especially for desilicated sample. Since, the catalytic activity and selectivities of hierarchical analogues are thought to be ruled by microporous environment (confinement effect for *n*-decane) and Brønsted acidity the observed drop of catalytic performance is justified for samples steamed at 700 °C.

Summing up, the native material appeared to be the most stable material against steaming in the cracking of *n*-decane. The removal both of Si and Al atoms by alkaline leaching, then subsequent reinsertion of aluminium atoms on the surface of led to a drop of the total acid strength of protonic sites in desilicated zeolites. Additionally, the protonic sites formed by reinsertion of Al atoms were prone to the formation of extraframework aluminium species by steaming process. This lower thermal stability was straightforwardly detected with the pyridine sorption. The concentration of the Lewis acid sites originating from extraframework species was even threefold higher for the alkaline leached zeolites than for native material. On the other hand, the increase of the accessibility of acid sites upon desilication facilitated the diffusion of *n*-decane but it did not affect the activity at all. Thus, catalytic activity in the cracking of *n*-decane is not ruled by the accessibility of centers, it directly reflects the acidic properties of the zeolite, particularly the acid strength of sites.

3.4.2 Cracking of TIPB: the role of mesoporous acidity

The activity of zeolite samples in cracking of TIPB molecules, which are not able to penetrate the 10-MR channels is expected to reveal the differences in accessibility of acid sites on the catalysts surface. The influence of differences in intrinsic Brønsted acidity on catalytic cracking will be discussed with regard to cracking reaction of *n*-decane, which is able to diffuse through the complete system of channels therefore is more demanding on the concentration and the strength of acid sites.

The comparison of reaction rate constants of TIPB cracking points to significant increase of catalytic activity of desilicated materials in the contrast to the native zeolite. The increase of the k_{TIPB} value is directly related to enhancement of the mesopores surface upon desilication (Table 8). The highest k_{TIPB} value is observed for zeolite D_NaOH&TBAOH/ZSM-5 and, moreover, it is found to be twice higher than for native ZSM-5. In spite of the drop of acid strength of sites after desilication, the fabrication of the secondary system of mesopores leads to higher accessibility of protonic sites. From the fact that catalytic activity of desilicated zeolites increased with the accessibility of protonic sites it could be anticipated that the mesopores system benefited the diffusion of the bulky 1,3,5-tri-isopropylbenzene molecule and, finally, provided higher activity of hierarchical zeolites. Therefore, not acidity of protonic sites but their enhanced accessibility is evidenced as the predominant factor influencing the TIPB cracking. It has to be remarked that the mesoporous samples, especially D_NaOH&TBAOH/ZSM-5 presents very high activity for the cracking of TIPB despite the presence of occluded mesoporosity as indicated by the nitrogen adsorption isotherms. This occluded mesoporosity, when reported for the conversion of methanol to hydrocarbons [29] did not improve lifetime and was attributed to the quality of mesopores that only could be reached by the reactants through the micropores. In the case of this contribution, for the cracking of TIPB, very sensitive to the presence of mesopores, the mesoporosity is very active, indicating that at least part of the mesoporosity is fully accessible at the reaction temperatures of cracking (500 ^{o}C) probably because are higher than those used for the methanol to hydrocarbon reaction (400-450 ^{o}C).

Steaming process (both at 650 ^{o}C and 700 ^{o}C) leads to a small decrease of the values of reaction rate constants k_{TIPB} for hierarchical zeolites (D_NaOH/ZSM-5 vs. S&D_NaOH/ZSM-5 and D_NaOH&TBAOH/ZSM-5 vs. S&D_NaOH&TBAOH/ZSM-5) – Table 8. A similar effect is observed for the native zeolite ZSM-5. Nevertheless, in spite of the fall in the value of the k_{TIPB} constant after steaming process, the hierarchical materials still exhibit significantly higher activity over non-steamed zeolite ZSM-5, and this advantage was particularly marked for NaOH&TBAOH-treated zeolite. This should be attributed to the preservation of the mesoporosity after steaming. Again, the substantial role of the enhanced accessibility of protonic sites (via generation of mesoporosity) is confirmed by higher activity of steamed hierarchical zeolites even though their protonic acidity is found to be lower than for non-steamed materials. An important finding is that the zeolite treated with NaOH&TBAOH shows not only

the highest conversion but, moreover, the highest selectivity to propene regardless the severity of the steaming process (Fig. 9). In addition, a direct result of desilication was lower coking tendency observed for hierarchical zeolites, which elongated the time-life of the catalyst. Also in this case, zeolite treated with NaOH&TBAOH appeared to be the most effective. This huge advantage of zeolites leached with alkaline solutions, over native material results from both the mesopores surface enhancement and the maintained stability of mesopores during the steaming process as well. This expanded system of mesopores affects the behaviour of the catalysts in both of these aspects. First of all, the enhancement of mesopores surface is related to an increase of the amount of silanol groups Si-OH (Fig. 6), which obviously possess acidity high enough to crack TIPB. Additionally, the active centers in the structure of hierarchical zeolite become accessible for bulky TIPB molecule. Both these factors are responsible for the high catalytic activity of desilicated zeolites. It has been reported that in AlMCM-41 the narrower diameter of mesopores was decisive factor for the stronger adsorption of 1,3,5-tri-isopropylbenzene on the mesopore wall leading to its higher catalytic activity in the TIPB cracking [38]. Thus, due to the confinement effect described above, the NaOH&TBAOH treated zeolite with system of mesopores of narrow diameters demonstrated significantly higher catalytic cracking activity over zeolite leached with NaOH only. Similar trends have been reported for the NaOH&TBAOH treated mordenites [39].

When looking at different selectivities at constant conversion, the hierarchical materials, both non- and steamed, present a lower amount of dry gas ($C_1 + C_2$) and higher olefinicity in the $C_{3=}/C_3$, $C_{4=}/C_4$, $iC_{4=}/iC_4$ ratios (Figure 9). Furthermore, the desilicated zeolites independently from thermal treatment (fresh, steamed at 650 °C or 700 °C), exhibited a slightly lower tendency for hydrogen-transfer reactions (HT), which is reflected as an increase of $C_{3=}/C_3$, $C_{4=}/C_4$, $iC_{4=}/iC_4$ ratios. – does it relate to the lower acidity of desilicated samples? What about the changes in C1+C2/isobutane and C3/C4 (higher values for desilicated samples)? The C4 products are secondary in case of TIPB cracking – but the ratio of C3/C4 increases for desilicated samples. So this trend should be opposite, right?

Comentado [LMT1]: The higher olefinicity is due to a lower extend of secondary hydrogen transfer reactions, which are decreased by the higher external surface of hierarchical materials. C1+C2/isobutane and C3/C4 are also higher for desilicated samples for the same reason as C4 comes from the secondary reactions of oligomerization-cracking of propylene as primary product.

3.4.3 Cracking of gasoil

Catalytic activity tests of the cracking of vacuum gasoil (Table 8), which were performed on desilicated zeolites MFI with the use reagents of various degree of branching, allowed the evaluation of the specific surface area of both micro-and mesopores, the influence of the acid properties and, finally, the potential application of hierarchical zeolites in gasoil cracking.

Comparison of reaction rate constants of vacuum gasoil cracking evidences that catalytic activity of desilicated materials and the parent zeolite remains on the same level (Fig. 10). It suggests that weaker acid strength of protonic sites in desilicated zeolites is balanced by highly enhanced accessibility of acid

sites related to the secondary system of mesopores in alkaline leached zeolites. Interesting correlation is driven for steamed zeolites. In this case the reaction rate constants of gasoil cracking held significantly high values (Table 8). Small decrease is observed, but extend of this change is considerably lower that for n-decane cracking. It can be reasonably correlated to the kinetic reaction rate constants for TIPB cracking. It clearly evidences the influence of the generated mesoporosity on the higher activity in diesel oil cracking of steamed hierarchical zeolites.

More differences were observed in the olefinicity ratios ($C_{3=}/C_3$, $C_{4=}/C_4$, $iC_{4=}/iC_4$). The non-steamed desilicated materials with higher external surface presents higher propylene/propane and butene/butane ratios that can be attributed to their lower tendency for hydrogen-transfer reactions (HT). In addition, the desilicated samples independently from thermal treatment presented higher value of $iC_{4=}/iC_4$ ratio that also confirms the higher accessibility of the framework that was not shown by the cracking of n-decane. It points that the vacuum gasoil preferentially undergoes transformation on the external surface of zeolite grains. As mentioned in the cracking of TIPB the dry gas yields were reduced for the hierarchical zeolites, both non-steamed and steamed. Thus, the lower values of both $(C_1 + C_2)$/isobutane and C_3/C_4 ratios in VGO cracking can be an indication of the pronounced occurrence of β-scission over protolytic cracking mechanisms on the mesoporous zeolites.

Comentado [LMT2]: Hydrogen transfer is a secondary reaction favored by long reactions paths as those of the native sample, while for the hierarchical materials primary reactions dominate as in the case of TIPB cracking.

Comentado [LMT3]: This is true, the mechanism is somehow different from that of TIPB, which reacts only by dealkylation to propylene that undergoes to oligomerization-cracking or hydrogen transfer. In the case of gasoil, with a mixture of bulky alkylaromatics and paraffins, protolytic cracking on the paraffins can occur with reaction (to C1-C2 or light paraffins + olefins)

4 CONCLUSIONS

Under conditions relevant for industrial FCC cracking process the application of ZSM-5 zeolite should be considered in terms of extensive in-situ dealumination by steaming. In order to investigate the changes in the acidity feature and catalytic performance the high silica hierarchical ZSM-5 zeolites were chosen as most suitable offering high stability in steaming conditions.

High silica zeolites desilicated by NaOH and NaOH&TBAOH leaching showed good hydrothermal stability against steaming with slightly lower resistance when comparing to native steamed zeolite. The mesoporosity was preserved after steaming. The influence of the generated mesoporosity on the higher activity was evidenced in both 1,3,5-tri-isopropylbenzene and gasoil cracking of steamed hierarchical zeolites. The zeolites with secondary system of mesopores were found to be of higher coking-resistance than pure microporous zeolite. Thus, in spite of lowered acidity, the mesopores system benefited the diffusion of the bulky molecule and finally provided higher activity of hierarchical zeolites.

ACKNOWLEDGMENTS

This work was financed by Grant No. 2015/18/E/ST4/00191 from the National Science Centre, Poland. F. Rey and J. Martinez-Triguero thank for the support of the Spanish Government-MINECO through ''Severo Ochoa" (SEV 2012-0267), MAT2015-71842-P and CTQ2015-68951-C3-1-R.

AUTHOR CONTRIBUTIONS

The manuscript was written through contributions of all authors. All authors have given approval to the final version of the manuscript.

REFERENCES

[1] K. Krishna, G.B.F. Seijer, C.M. van den Bleek, H. van Bekkum, H.P.A. Calis, Chem. Commun., (2002) 948.

[2] X. Gao, X. Zou, F. Zhang, S. Zhang, H. Ma, N. Zhao, G. Zhu, Chem. Commun., 49 (2013) 8839.

[3] C.S. Cundy, P.A. Cox , Chem. Rev., 103 (2003) 663.

[4] Y. Kamimura, Ch. Kowenje, K. Yamanaka, K. Itabashi, A. Endo, T. Okubo, Microporous and Mesoporous Mater., 181 (2013) 154.

[5] K. Egeblad, C.H. Christensen, M. Kustova, CH. Christensen, Chem. Mater., 20 (2008) 946.

[6] J.C. Groen, J.A. Moulijn, J. Perez-Ramirez, J. Mater. Chem., 16 (2006) 2121.

[7] J. Pérez-Ramírez, C.H. Christensen, K. Egeblad, C.H. Christensend, J.C. Groen, Chem. Soc. Rev., 37 (2008) 2530.

[8] R. Chal, C. Grardin, M. Bulut, S. van Donk, Chem. Cat. Chem., 3 (2011) 67.

[9] K. Cho, H.S. Cho, L.C. de Menorval, R. Ryoo, Chem. Mater., 21 (2009) 5664.

[10] C. Mei, P. Wen, Z. Liu, Y. Wang, W. Yang, Z. Xie, W. Hua, Z. Gao, J. Catal., 258 (2008) 243.

[11] D. Verboekend, J.C. Groen, J. Pérez-Ramirez, Adv. Funct. Mater., 20 (2010) 1441.

[12] J.C. Groen, T. Sano, J.A. Mouljin, J. Pérez-Ramirez, J. Catal., 251 (2007) 21.

[13] J. Peréz-Ramírez, D. Verboekend, A. Bonilla, S. Abelló, Adv. Funct. Mater., 19 (2009) 3972.

[14] D. Verboekend, J. Pérez-Ramirez, Chem. Eur. J., 17 (2011) 1137.

[15] X. Li, D.F. Shantz, J. Phys. Chem. C. 114 (2010) 8449.

[16] Y. Zhu, Z. Hua, J. Zhou, L. Wang, J.Zhao, Y. Gong, W. Wu, J. Shi, Chem. Eur. J., 17 (2011) 14618.

[17] N.S. Nesterenko, F. Thibault-Starzyk, V. Montouillout, V.V. Yuschenko, C. Fernandez, J.-P. Gilson, F. Fajula, I.I. Ivanova, Micropor. Mesopor. Mater., 71 (2004) 157.

[18] T. Montanari, M. Bevilacqua, G. Busca, Appl. Catal. A, 307 (2006) 21.

[19] K. Sadowska , K. Góra-Marek, J. Datka, J. Phys. Chem. C, 117 (2013) 9237.

[20] G. Busca, Chem. Rev., 107 (2007) 5366.

[21] J. Ding, H. Liu, P. Yuan, G. Shi, X. Bao, ChemCatChem, 5 (2013) 2258.

[22] J. Buchanan, Catal. Today, 55 (2000) 207.

[23] K. Sadowska, K. Góra-Marek, J. Datka, Vib. Spectrosc., 63 (2012) 418.

[24] A. Corma, J. Martínez-Triguero, Appl. Catal. A. General 118 (1994) 153.

[25] A. Corma, F. Melo, J. Prieto, PES 2 011 993, 1989.

[26] J. Pérez-Ramírez, D. Verboekend, A. Bonilla, S. Abelló, Adv. Funct. Mater., 19 (2009) 3972.

[27] K. Sadowska, A. Wach, A., Z. Olejniczak, P. Kuśtrowski, J. Datka, Microporous and Mesoporous Mater., 167 (2013) 82.

[28] M. Milina, S. Mitchell, D. Cooke, P. Crivelli, J. Pérez-Ramírez, Angew. Chem. Int. Edi., 54 (2015) 1591.

[29] M. Milina, S. Mitchell, P. Crivelli, D. Cooke, J. Pérez-Ramírez, Nature Comm. 2014, 5.

[30] R. Otomo, T. Yokoi, J.N. Kondo, T. Tatsumi, Appl. Catal. A, 470 (2014) 318.

[31] L. H. Ong, M. Dömök, R. Olindo, A. van Veen, J.A. Lercher, Microporous and Mesoporous Mater., 164 (2012) 9.

[32] A. Bonilla, D. Baudouin, J. Pérez-Ramírez, J. Catal., 265 (2009) 170.

[33] T. Blasco, A. Corma, J. Martínez Triguero, J. Catal., 237 (2006) 267.

[34] R. Rachwalik, Z. Olejniczak, J. Jiao, J. Huang, M. Hunger, B. Sulikowski, J. Catal. 252 (2007) 161.

[35] J.A. Ripmeester, A. Majid, R.E. Hawkins, J. Inclusion Phenom., 1 (1983) 193.

[36] A. Corma, P. J. Miguel, A. V. Orchille, Appl. Catal. A., 117 (1994) 29.

[37] B. Xu, C. Sievers, S.B. Hong, R. Prins, J.A. van Bokhoven, J. Catal., 244 (2006) 163.

[38] W.-H. Chen, S.-J. Huang, Q. Zhao, H.-P. Lin, C.-Y. Mou, S.-B. Liu, Top. Catal., 52 (2009) 2.

[39] K. Góra-Marek, K. Tarach, J. Tekla, Z. Olejniczak, P. Kuśtrowski, L. Liu, J. Martinez-Triguero, F. Rey, J. Phys. Chem. C 48 (2014) 28043.

Figures Captions

Figure 1. The schematic representation of modifications and treatments performed on studied zeolites.

Figure 2. XRD patterns of native ZSM-5 and desilicated zeolites D_NaOH/ZSM-5 and D_NaOH&TBAOH/ZSM-5.

Figure 3. The N_2 adsorption-desorption isotherms and BJH pore size distribution for parent and desilicated materials.

Figure 4. TEM micrographs (200 nm) of native ZSM-5 and desilicated zeolites D_NaOH/ZSM-5 and D_NaOH&TBAOH/ZSM-5.

Figure 5. The ^{27}AlMAS NMR spectra of studied materials.

Figure 6. The spectra of OH groups of studied materials.

Figure 7. The changes of the Brønsted and Lewis acid sites' concentration in modified hierarchical zeolites.

Figure 8. Total conversion and selectivities in the cracking of *n*-decane at 500 °C and 60 s time on stream over (a) fresh, (b) steamed at 650 °C and (c) steamed at 700 °C parent and hierarchical zeolites.

Figure 9. Total conversion and selectivities in the cracking of TIPB at 500 °C and 60 s time on stream over (a) fresh, (b) steamed at 650 °C and (c) steamed at 700 °C parent and hierarchical zeolites.

Figure 10. Total conversion and selectivities in the cracking of VGO at 520 °C and 30 s time on stream over (a) fresh, (b) steamed at 650 °C and (c) steamed at 700 °C parent and hierarchical zeolites.

Table 1. The samples used in the study.

Sample name	Sample symbol	Preparation of sample
Native	ZSM-5	-
After reaction	R/ZSM-5	Native zeolite ZSM-5 tested as catalyst in the cracking VGO
Steamed native	S650/ZSM-5 S700/ZSM-5	The ZSM-5 zeolite was preheated form RT to steaming temperature during 2 hours. Steaming was performed in 650 ^{o}C and 700 ^{o}C under continuous water injection with 1.8 cm^3min^{-1} flow speed for 3 hours.
Desilicated with NaOH	D_NaOH/ZSM-5	The 100 ml of 0.2 M NaOH solution was contacted with 3.0 g of zeolite at 65 ^{o}C for half an hour.
After reaction	R/D_NaOH/ZSM-5	NaOH-desilicated zeolite ZSM-5 tested as catalyst in the cracking VGO
Steamed desilicated with NaOH	S650&D_NaOH/ZSM-5 S700&D_NaOH/ZSM-5	The D_NaOH/ZSM-5 catalyst was preheated form RT to steaming temperature during 2 hours. Steaming was performed in 650 ^{o}C and 700 ^{o}C under continuous water injection with 1.8 cm^3min^{-1} flow speed for 3 hours.
Desilicated with NaOH&TBAOH	D_NaOH&TBAOH/ZSM-5	The 100 ml of 0.2 M NaOH&TBAOH solution was contacted with 3.0 g of zeolite at 65 ^{o}C for half an hour. 0.2 M mixture TBAOH/(NaOH+TBAOH) ratio was 0.4.
After reaction	R/D_NaOH&TBAOH/ZSM-5	NaOH TBAOH-desilicated zeolite ZSM-5 tested as catalyst in the cracking VGO
Steamed desilicated with NaOH&TBAOH	S650&D_NaOH&TBAOH/ZSM-5 S700&D_NaOH&TBAOH/ZSM-5	The D_NaOH&TBAOH/ZSM-5 catalyst was preheated form RT to steaming temperature during 2 hours. Steaming was performed in 650 ^{o}C and 700 ^{o}C under continuous water injection with 1.8 cm^3min^{-1} flow speed for 3 hours.

Table 2. The conditions of catalytic cracking reactions for different feeds

Reagent	Reaction conditions
***n*-decane**	Temperature of reaction: 500 °C; TOS = 60 s; catalyst: 300 mg, fraction 0.59–0.84 mm + 2.5 g SiO_2, fraction 0.2-0.4 mm
TIPB (1,3,5-triisopropylbenzene)	Temperature of reaction: 500 °C; TOS = 60 s; catalyst: 300 mg, fraction 0.59–0.84 mm
Vacuum gas oil (VGO)	Temperature of reaction: 520 °C; TOS = 30 s; catalyst: 500 mg, fraction 0.59–0.84 mm + 2.5 g SiO_2, fraction 0.2-0.4 mm

Table 3. Reference VGO feedstock properties.

Parameters	Values
density (15 °C)	0.9172 g/cm^3
aniline point (°C)	79.2
sulphur (%)	1.65
N_2 (ppm)	1261
Na (ppm)	0.18
Cu (ppm)	<0.1
Fe (ppm)	0.30
Ni (ppb)	0.2
V (ppb)	0.40
ASTM D-1160 (◦C)	
5%	319
10%	352
30%	414
50%	436
70%	459
90%	512
Average molecular weight	407
aromat. carb. (ndM%)	22.96
naphten carb. (ndM%)	15.16
paraff. carb. (ndM%)	61.88
arom. rings./molec. (ndM)	1.17
napht. rings./molec. (ndM)	1.01

Table 4. The composition of the studied zeolites determined by chemical analysis (Si/Al), the % of crystallinity calculated from XRD patterns and textural parameters from low temperature N_2 adsorption for studied materials.

Zeolite	Si/Al	% Cryst.	S_{BET}	S_{meso}	V_{micro}	V_{meso}
			[m^2g^{-1}]		[cm^3g^{-1}]	
ZSM-5	164	100	373	335	0.16	0.25
R/ZSM-5			364	323	0.16	0.24
S650/ZSM-5			380	339	0.16	0.25
S700/ZSM-5			370	331	0.16	0.24
D_NaOH/ZSM-5	124	92	394	311	0.15	0.40
R&D_NaOH/ZSM-5			383	302	0.15	0.39
S650&D_NaOH/ZSM-5			377	305	0.15	0.39
S700&D_NaOH/ZSM-5			364	294	0.15	0.39
D_NaOH&TBAOH/ZSM-5	124	88	419	280	0.14	0.44
R&D_NaOH&TBAOH/ZSM-5			418	275	0.14	0.43
S650&D_NaOH&TBAOH/ZSM-5			412	278	0.14	0.43
S700&D_NaOH&TBAOH/ZSM-5			382	262	0.13	0.44

Table 5. The concentration of Al atoms from chemical analysis, the concentration of Brønsted (B) and Lewis acid sites (L) from IR spectroscopy measurements with pyridine and pivalonitrile.

Zeolite	Al [µmol·g^{-1}]	Py [µmol·g^{-1}]			Pn [µmol·g^{-1}]	
		B	L	L+B	B	L
ZSM-5	94	85	7	92	25	0
R/ZSM-5		85	9	94	20	*bdl**
S650/ZSM-5		48	30	78	12	*bdl**
S700/ZSM-5		36	40	76	7	*bdl**
D_NaOH/ZSM-5	125	101	30	131	66	12
R&D_NaOH/ZSM-5		95	40	135	42	9
S650&D_NaOH/ZSM-5		48	93	141	24	9
S700&D_NaOH/ZSM-5		34	110	135	22	23
D_NaOH&TBAOH/ZSM-5	125	95	33	128	91	30
R&D_NaOH&TBAOH/ZSM-5		72	56	128	68	21
S650&D_NaOH&TBAOH/ZSM-5		34	57	91	30	20
S700&D_NaOH&TBAOH/ZSM-5		34	121	155	25	18

**below detection limit or determined with not sufficient confidence*

Table 6. Relative concentrations of Si and Al on external surface of zeolite grains and calculated Si/Al ratios (and Al concentrations) of surface and bulk for studied zeolites.

Zeolite	% Conc.		Surface		Bulk	
	% Si 2p	% Al 2p	Si/Al	Al/μmolg^{-1}	Si/Al	Al/μmolg^{-1}
ZSM-5	41.66	0.31	134	115	164	94
D_NaOH/ZSM-5	41.50	0.75	55	276	124	124
D_NaOH&TBAOH/ZSM-5	42.29	0.50	85	182	124	124

Table 7. Acid strength of Si(OH)Al groups obtained from (a) position of Si(OH)Al band expressed by ν_{OH}, (b) low temperature CO sorption expressed by $\Delta\nu_{O\text{-}H\cdots CO}$ as well as from (c) IR studies of pyridine thermodesorption expressed as $\frac{A_{500}}{A_{170}}$.

Zeolite	Si/Al	Strength of Brønsted acid centers		
		ν_{OH} /cm^{-1}	$\Delta\nu_{OH\cdots CO}$ /cm^{-1}	$\frac{A_{500}}{A_{170}}$
ZSM-5	164	3615	320	1.00
D_NaOH/ZSM-5	124	3610	310	0.85
D_NaOH&TBAOH/ZSM-5	124	3612	316	0.95

Table 8. First-order kinetic rate constants for *n*-decane ($k_{n\text{-}C10}$) and TIPB (k_{TIPB}) cracking reactions. Second-order kinetic rate constants for vacuum gas oil (k_{VGO}) cracking reactions.

Zeolite	$k_{n\text{-}C10}$	k_{TIPB}	k_{VGO}	Zeolites steamed at 650 °C	$k_{n\text{-}C10}$	k_{TIPB}	k_{VGO}	Zeolites steamed at 700 °C	$k_{n\text{-}C10}$	k_{TIPB}	k_{VGO}
	[10^{-2} s^{-1}]				[10^{-2} s^{-1}]				[10^{-2} s^{-1}]		
ZSM-5	0.95	1.49	1.03	**S650/ZSM-5**	0.58	1.32	0.89	**S700/ZSM-5**	0.61	1.14	0.87
D_NaOH/ZSM-5	0.77	2.63	1.06	**S650&D_NaOH/ZSM-5**	0.24	2.37	0.86	**S700&D_NaOH/ZSM-5**	0.27	1.76	0.86
D_NaOH&TBAOH/ZSM-5	0.82	3.61	1.15	**S650&D_NaOH&TBAOH/ZSM-5**	0.48	2.99	0.94	**S700&D_NaOH&TBAOH/ZSM-5**	0.17	3.03	0.79

Figure 1. Schematic representation of modifications and treatments performed on studied zeolites.

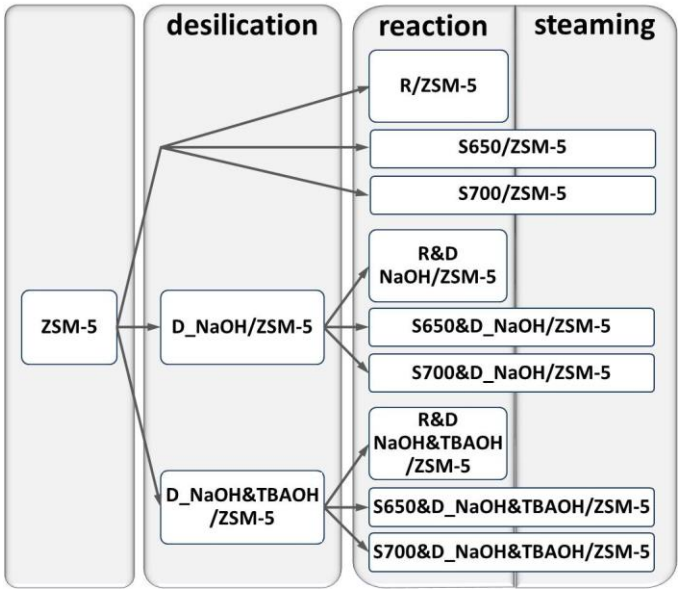

Figure 2. XRD patterns of native ZSM-5 and desilicated zeolites D_NaOH/ZSM-5 and D_NaOH&TBAOH/ZSM-5.

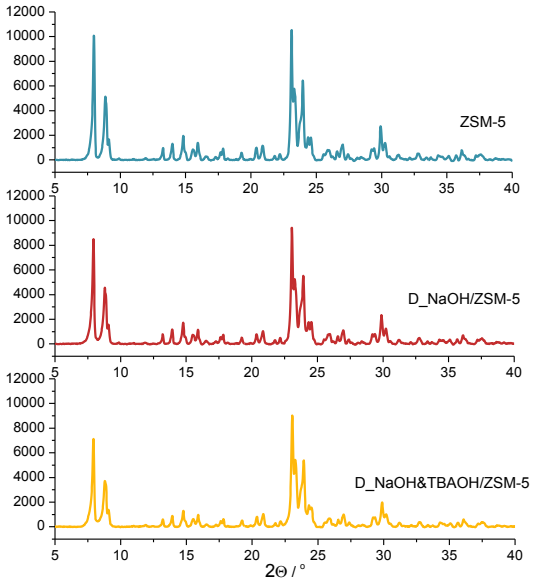

Figure 3. N_2 adsorption-desorption isotherms and BJH pore size distribution of parent and desilicated materials.

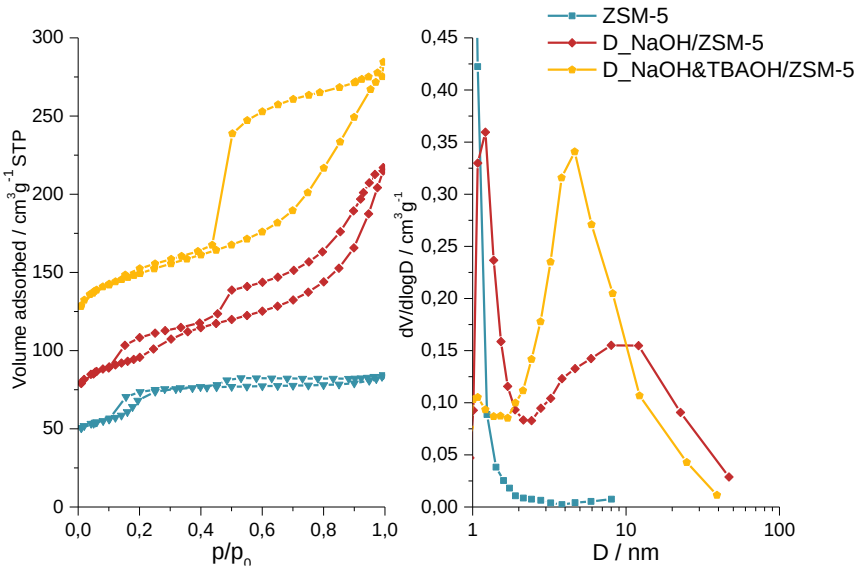

Figure 4. TEM micrographs (200 nm) of native ZSM-5 and desilicated zeolites D_NaOH/ZSM-5 and D_NaOH&TBAOH/ZSM-5.

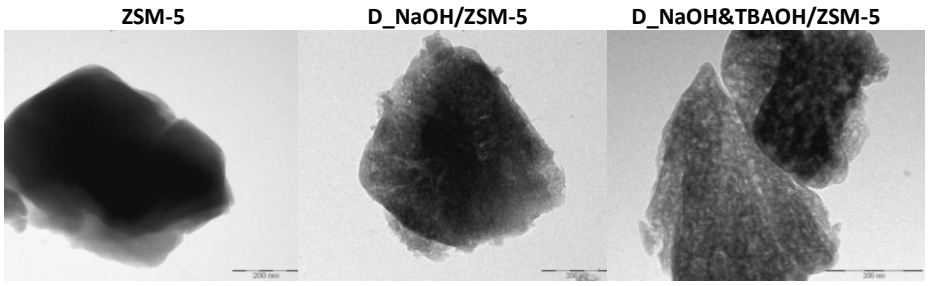

Figure 5. ^{27}Al MAS NMR spectra of studied materials.

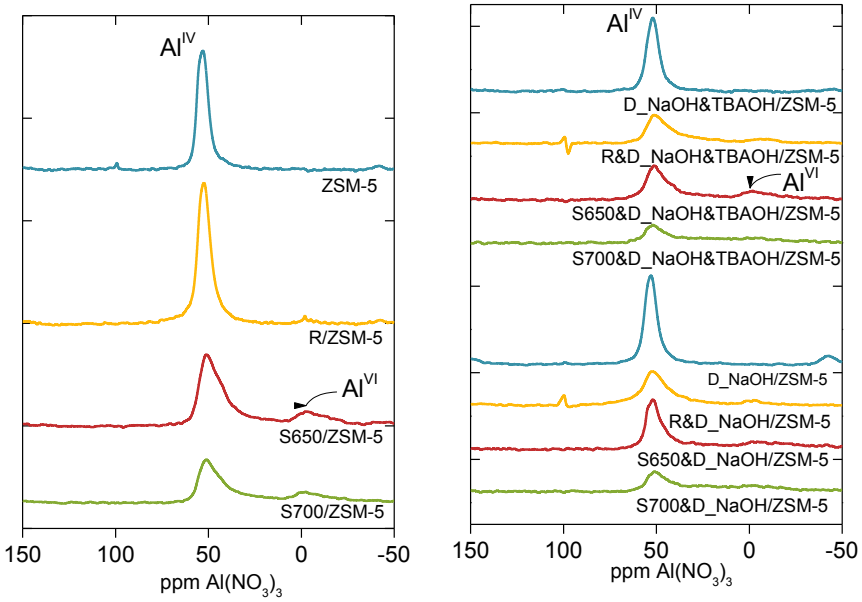

Figure 6. Spectra of OH groups of studied materials.

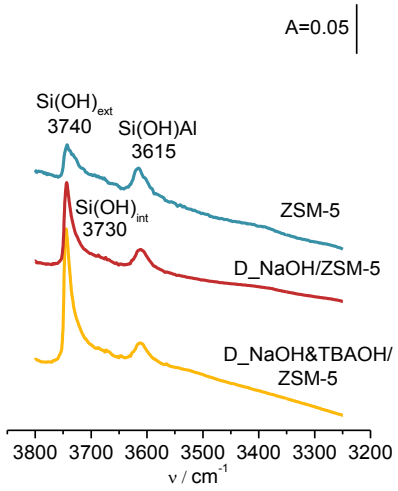

Figure 7. Changes of the Brønsted and Lewis acid sites concentration in modified hierarchical zeolites.

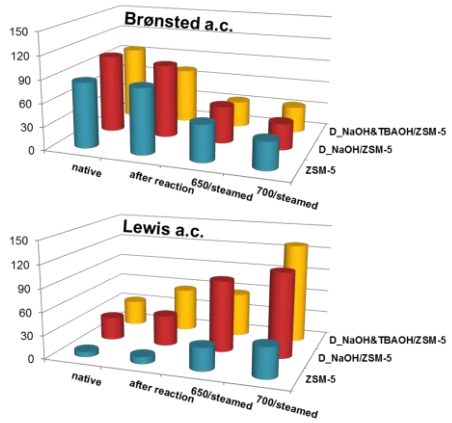

Figure 8. Total conversion and selectivities in cracking of *n*-decane at 500 °C and 60 s time on stream over (a) fresh, (b) steamed at 650 °C and (c) steamed at 700 °C parent and hierarchical zeolites.

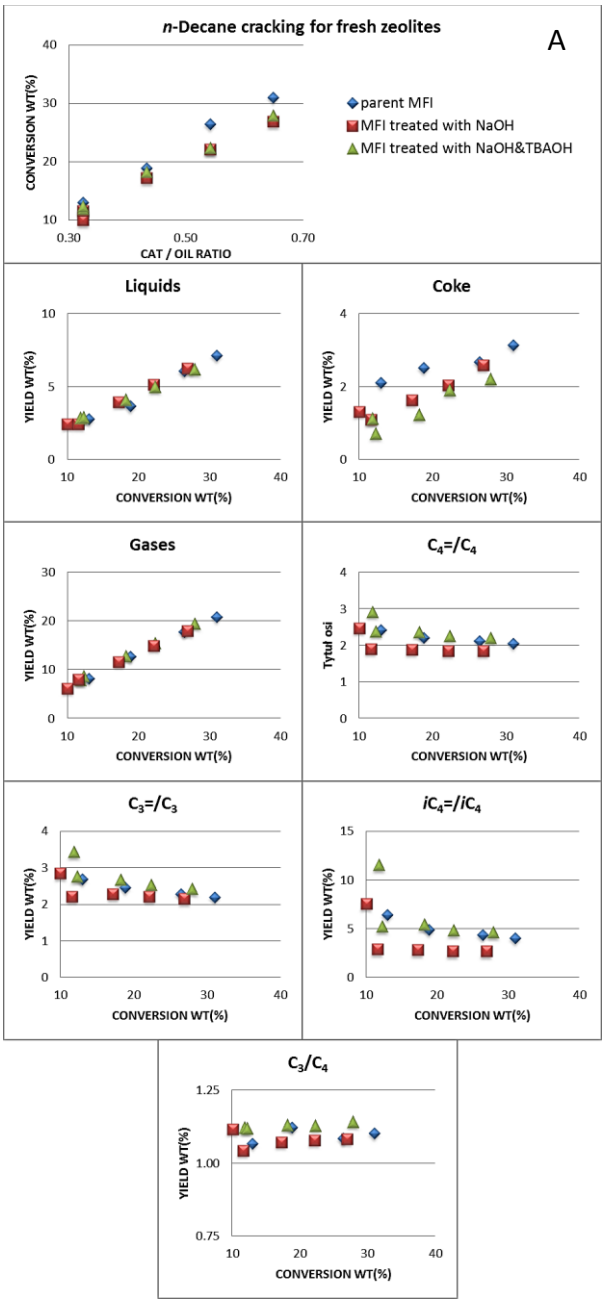
n-Decane cracking for fresh zeolites
A
CONVERSION WT(%)
CAT / OIL RATIO
parent MFI
MFI treated with NaOH
MFI treated with NaOH&TBAOH
Liquids
Coke
Gases
C4=/C4
C3=/C3
iC4=/iC4
C3/C4
YIELD WT(%)
Tytul osi
CONVERSION WT(%)

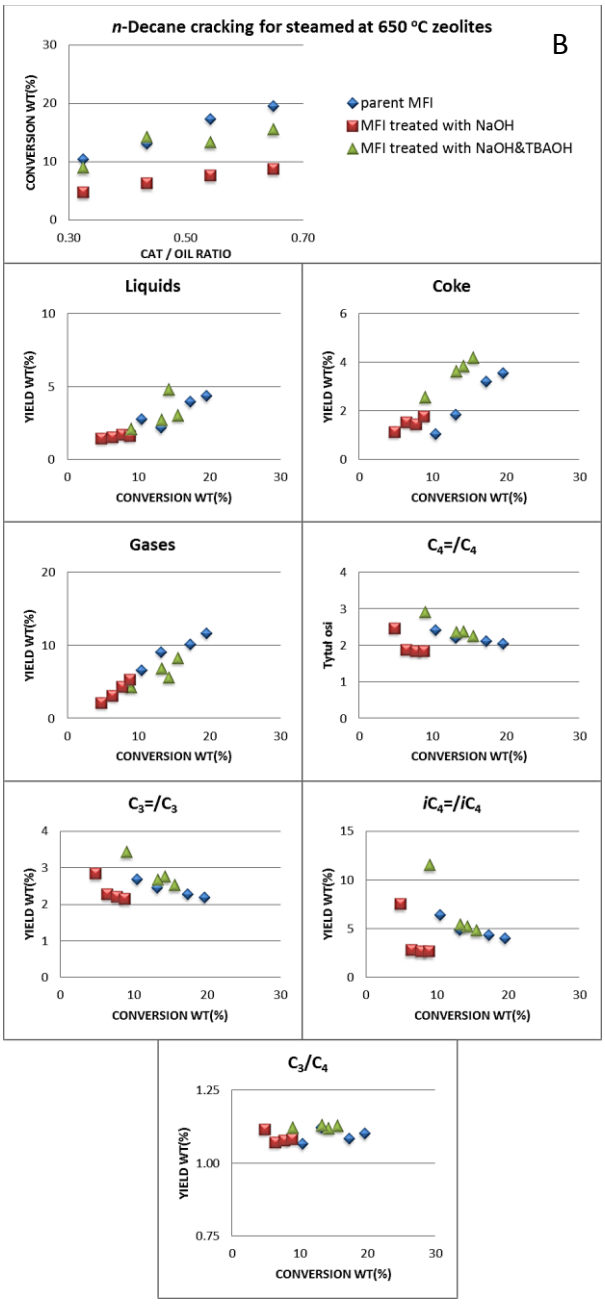
n-Decane cracking for steamed at 650 °C zeolites
B
CONVERSION WT(%)
CAT / OIL RATIO
parent MFI
MFI treated with NaOH
MFI treated with NaOH&TBAOH
Liquids
Coke
Gases
C4=/C4
C3=/C3
iC4=/iC4
C3/C4
YIELD WT(%)
Tytul osi
CONVERSION WT(%)

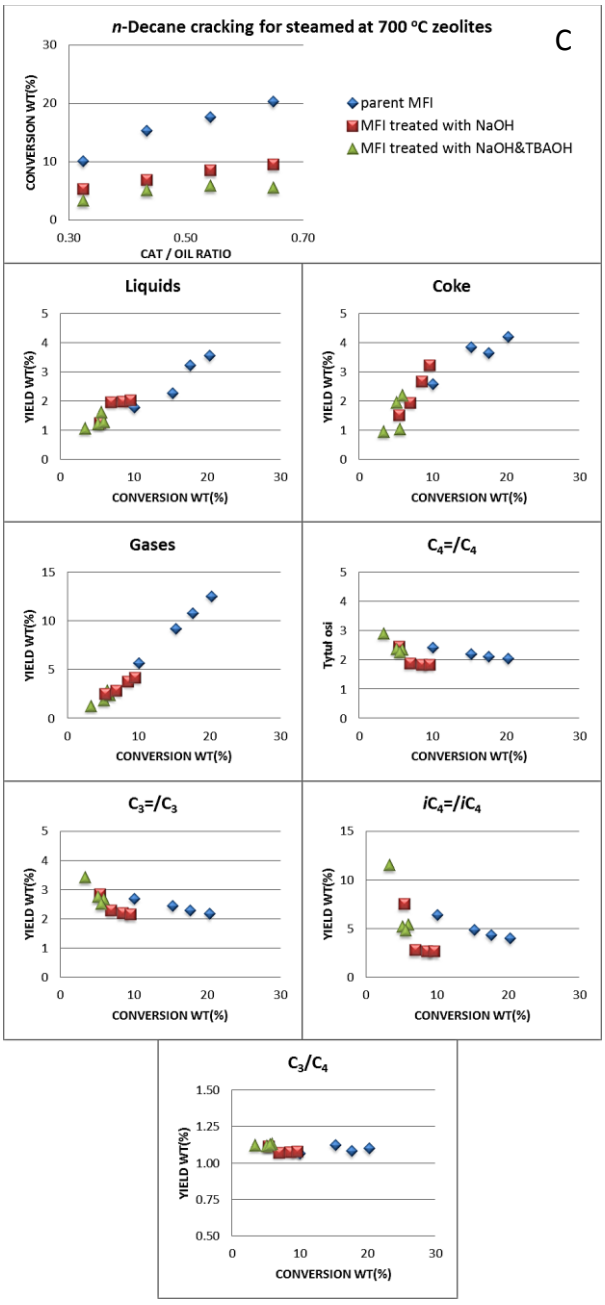
n-Decane cracking for steamed at 700 °C zeolites
C
CONVERSION WT(%)
CAT / OIL RATIO
parent MFI
MFI treated with NaOH
MFI treated with NaOH&TBAOH
Liquids
Coke
Gases
C4=/C4
C3=/C3
iC4=/iC4
C3/C4
YIELD WT(%)
Tytul osi
CONVERSION WT(%)

Figure 9. Total conversion and selectivities in the cracking of TIPB at 500 °C and 60 s time on stream over (a) fresh, (b) steamed at 650 °C and (c) steamed at 700 °C parent and hierarchical zeolite

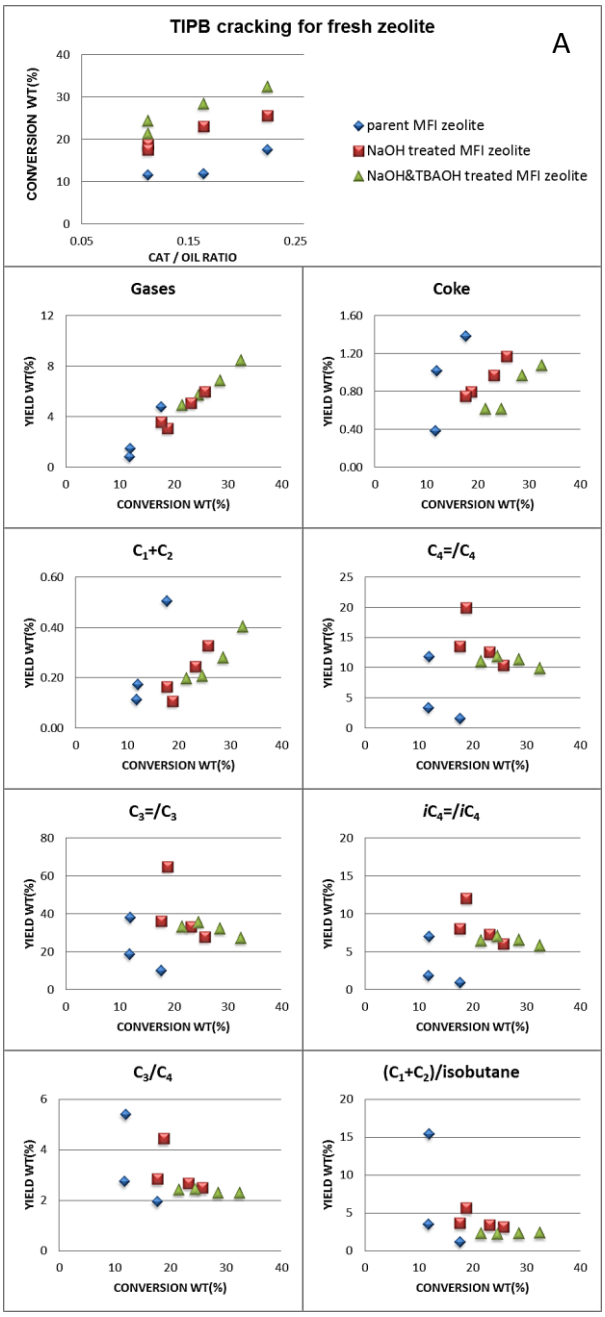

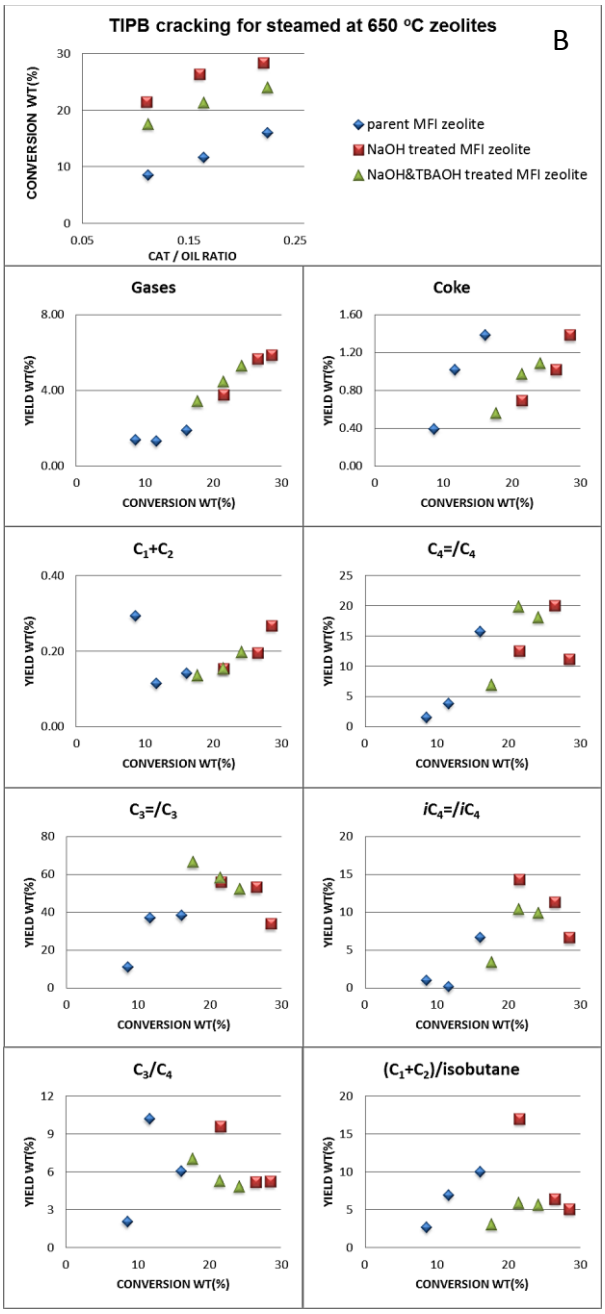
TIPB cracking for steamed at 650 °C zeolites
B
CONVERSION WT(%)
CAT / OIL RATIO
parent MFI zeolite
NaOH treated MFI zeolite
NaOH&TBAOH treated MFI zeolite
Gases
Coke
C_1+C_2
$C_4=/C_4$
$C_3=/C_3$
$iC_4=/iC_4$
C_3/C_4
(C_1+C_2)/isobutane
YIELD WT(%)
CONVERSION WT(%)

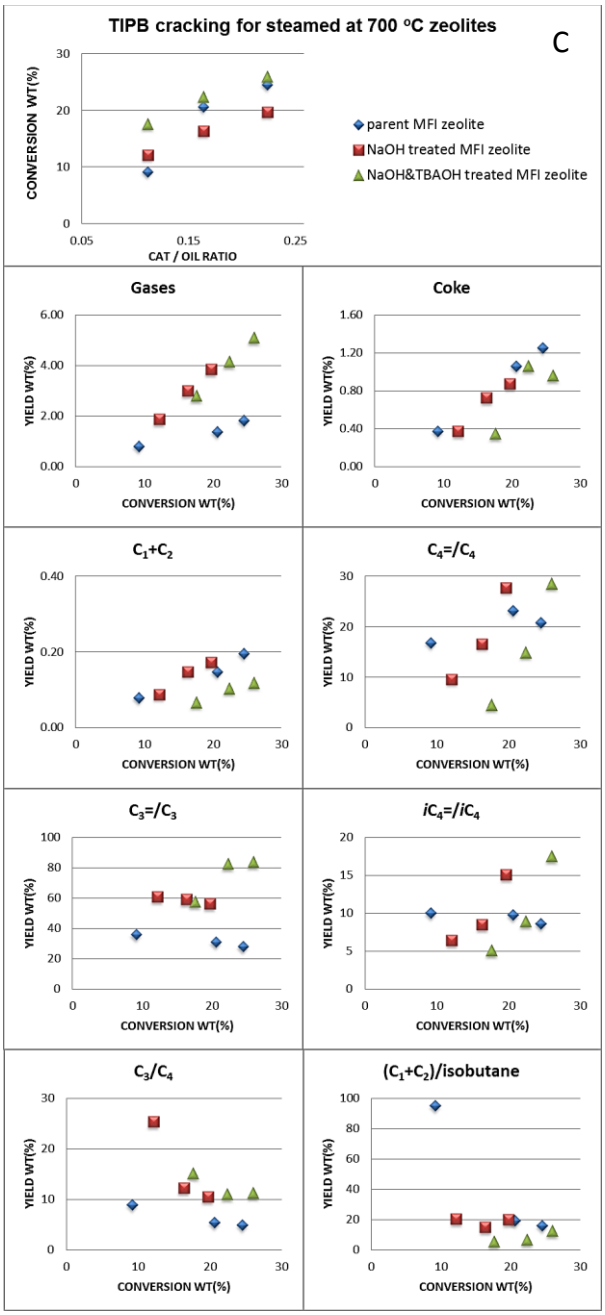
TIPB cracking for steamed at 700 °C zeolites
C
CONVERSION WT(%)
CAT / OIL RATIO
parent MFI zeolite
NaOH treated MFI zeolite
NaOH&TBAOH treated MFI zeolite
Gases
Coke
C_1+C_2
$C_4=/C_4$
$C_3=/C_3$
$iC_4=/iC_4$
C_3/C_4
(C_1+C_2)/isobutane
YIELD WT(%)
CONVERSION WT(%)

Figure 10. Total conversion and selectivities in the cracking of VGO at 520 °C and 30 s time on stream over (a) fresh, (b) steamed at 650 °C and (c) steamed at 700 °C parent and hierarchical zeolites.

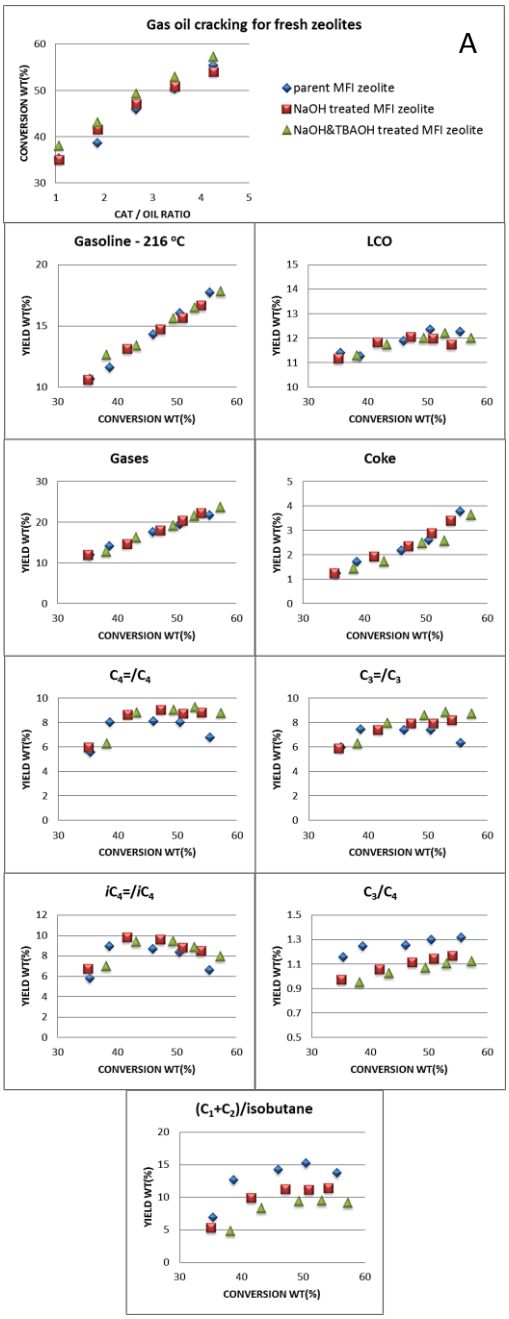

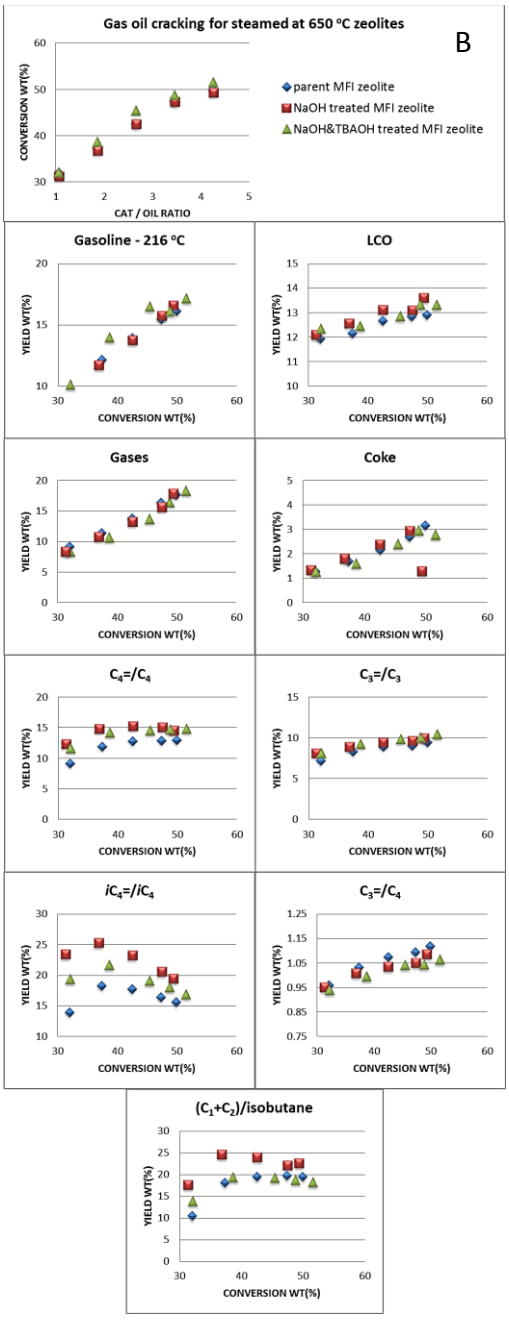
Gas oil cracking for steamed at 650 °C zeolites
B
CONVERSION WT(%)
CAT / OIL RATIO
parent MFI zeolite
NaOH treated MFI zeolite
NaOH&TBAOH treated MFI zeolite
Gasoline - 216 °C
LCO
Gases
Coke
C4=/C4
C3=/C3
iC4=/iC4
C3=/C4
(C1+C2)/isobutane
YIELD WT(%)
CONVERSION WT(%)

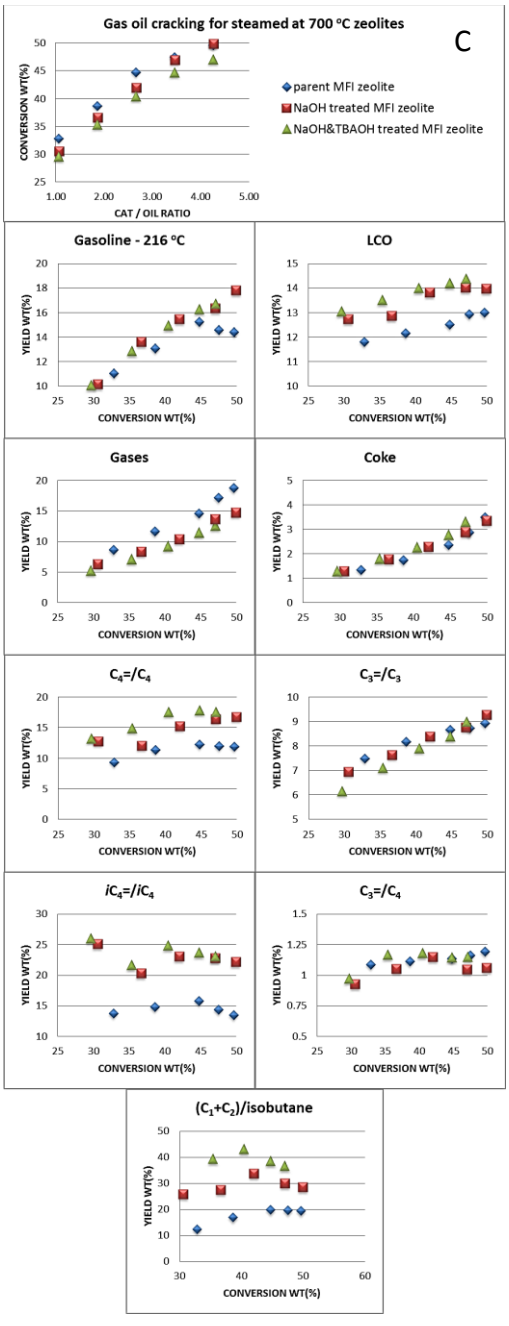
Gas oil cracking for steamed at 700 °C zeolites
C
parent MFI zeolite
NaOH treated MFI zeolite
NaOH&TBAOH treated MFI zeolite
CONVERSION WT(%)
CAT / OIL RATIO
Gasoline - 216 °C
LCO
Gases
Coke
C4=/C4
C3=/C3
iC4=/iC4
C3=/C4
(C1+C2)/isobutane
YIELD WT(%)
CONVERSION WT(%)

FIGURES IN BLACK-AND-WHITE

Figure 2. XRD patterns of native ZSM-5 and desilicated zeolites D_NaOH/ZSM-5 and D_NaOH&TBAOH/ZSM-5.

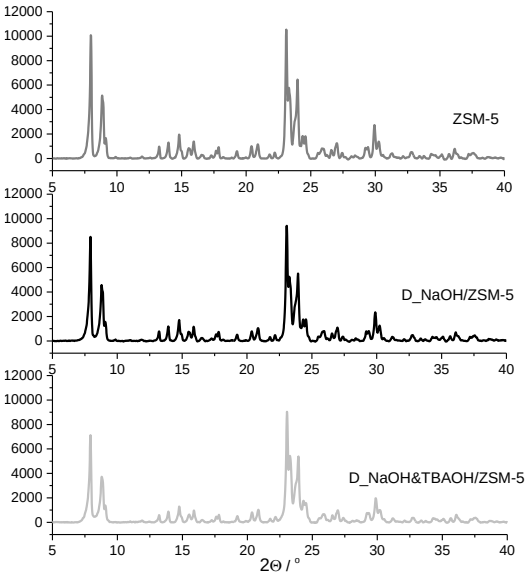

Figure 3. N_2 adsorption-desorption isotherms and BJH pore size distribution of parent and desilicated materials.

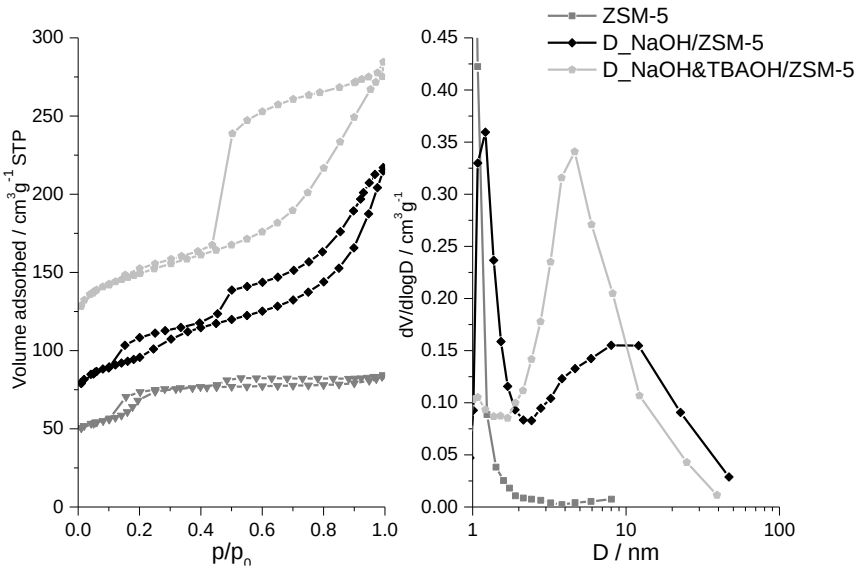

Figure 5. ^{27}Al MAS NMR spectra of studied materials.

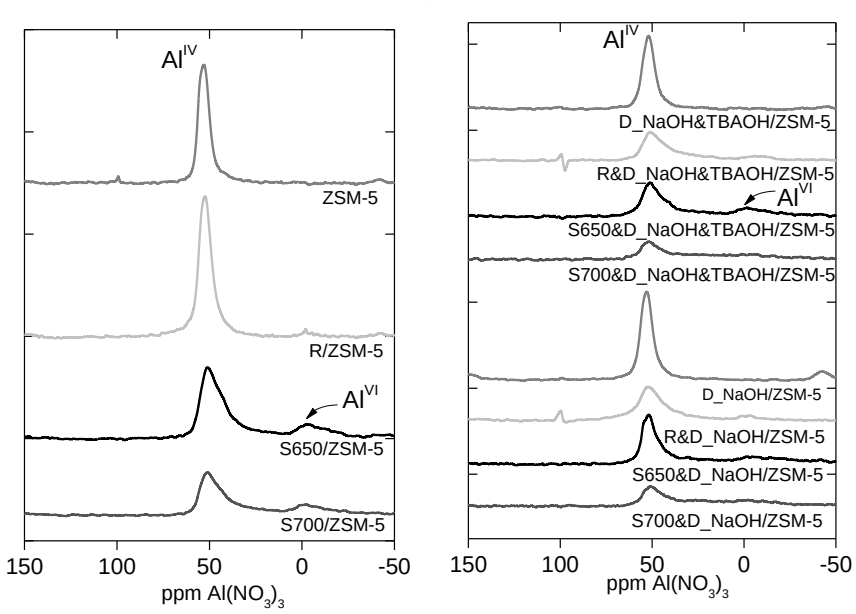

Figure 6. Spectra of OH groups of studied materials.

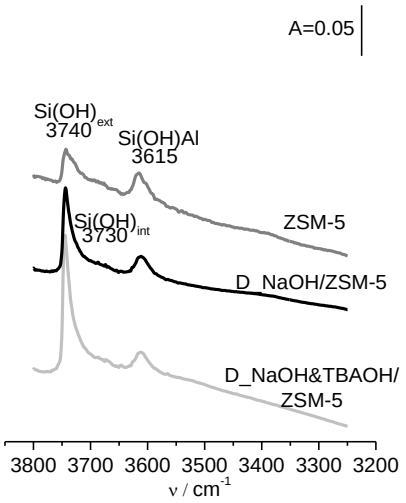

Figure 7. Changes of the Brønsted and Lewis acid sites concentration in modified hierarchical zeolites.

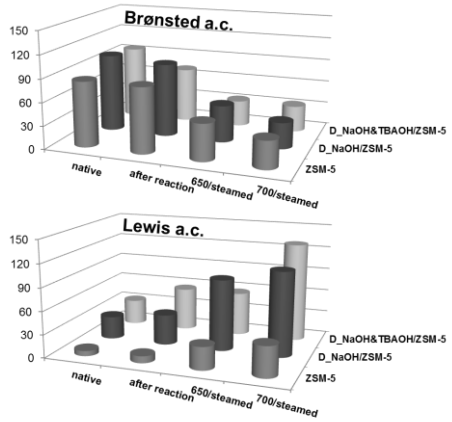

Figure 8. Total conversion and selectivities in cracking of *n*-decane at 500 °C and 60 s time on stream over (a) fresh, (b) steamed at 650 °C and (c) steamed at 700 °C parent and hierarchical zeolites.

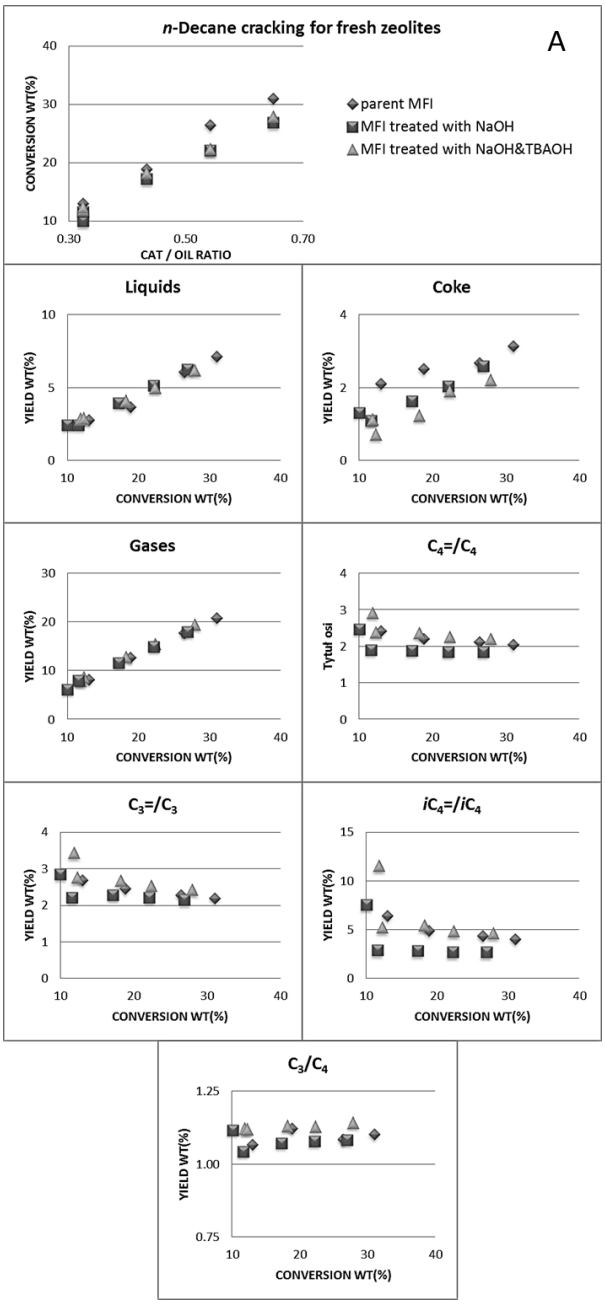

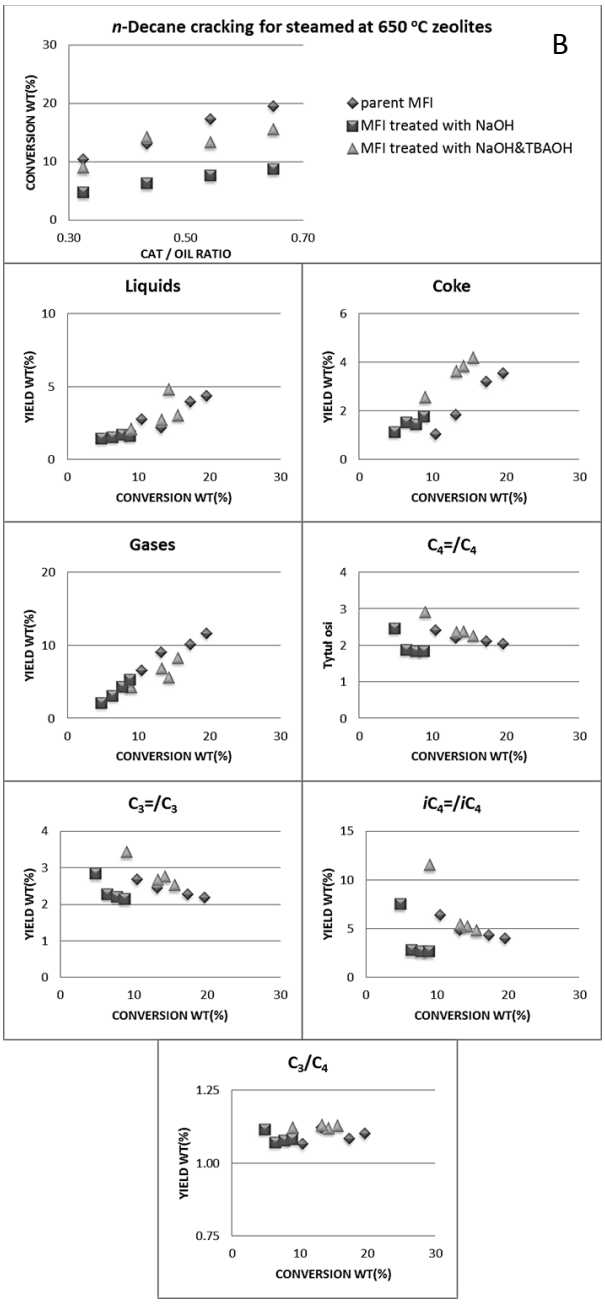
n-Decane cracking for steamed at 650 °C zeolites
B
CONVERSION WT(%)
CAT / OIL RATIO
parent MFI
MFI treated with NaOH
MFI treated with NaOH&TBAOH
Liquids
Coke
Gases
C4=/C4
C3=/C3
iC4=/iC4
C3/C4
YIELD WT(%)
Tytul osi
CONVERSION WT(%)

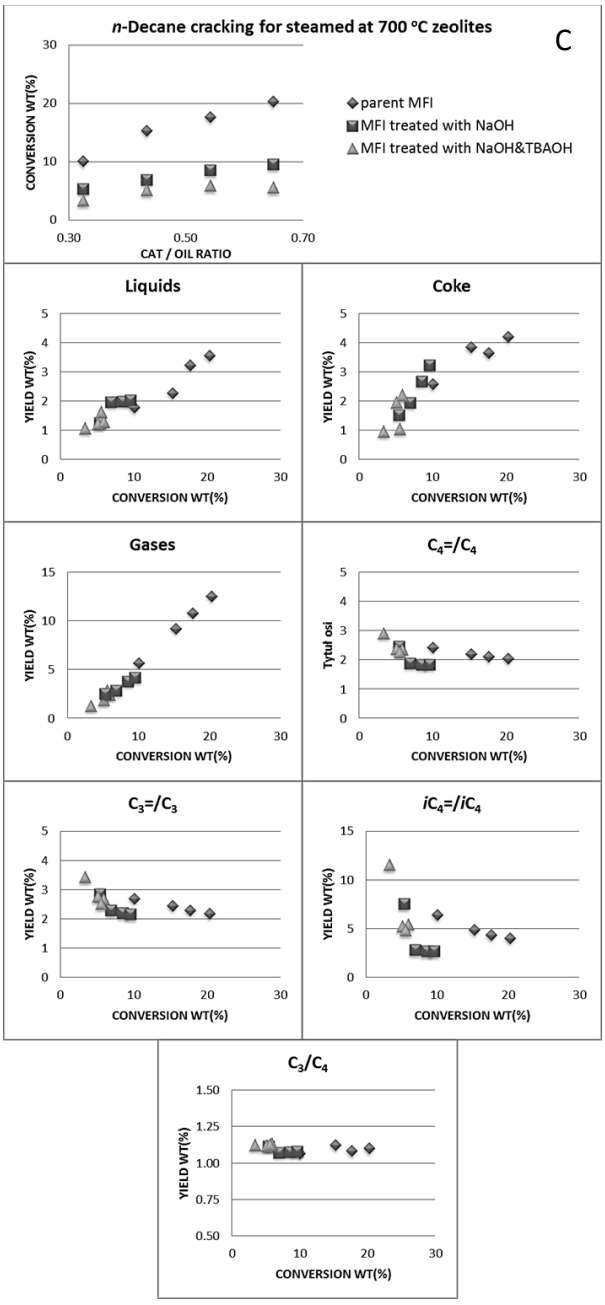
n-Decane cracking for steamed at 700 °C zeolites
C
CONVERSION WT(%)
CAT / OIL RATIO
parent MFI
MFI treated with NaOH
MFI treated with NaOH&TBAOH
Liquids
Coke
Gases
C4=/C4
C3=/C3
iC4=/iC4
C3/C4
YIELD WT(%)
Tytul osi
CONVERSION WT(%)

Figure 9. Total conversion and selectivities in the cracking of TIPB at 500 °C and 60 s time on stream over (a) fresh, (b) steamed at 650 °C and (c) steamed at 700 °C parent and hierarchical zeolite

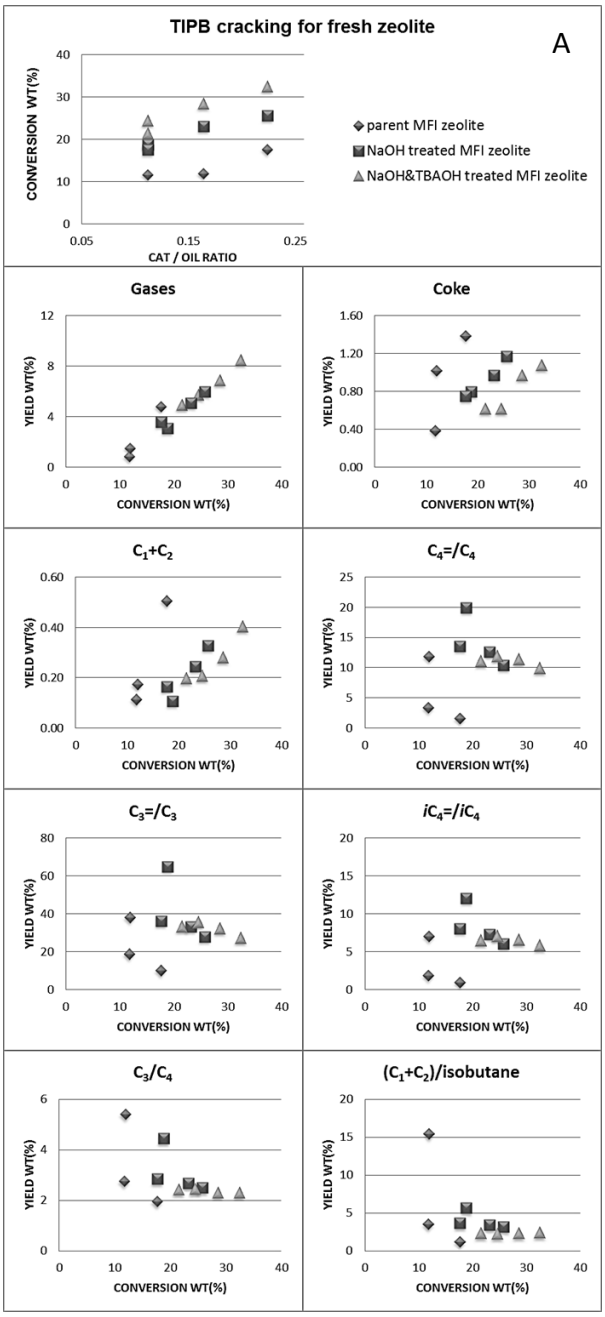

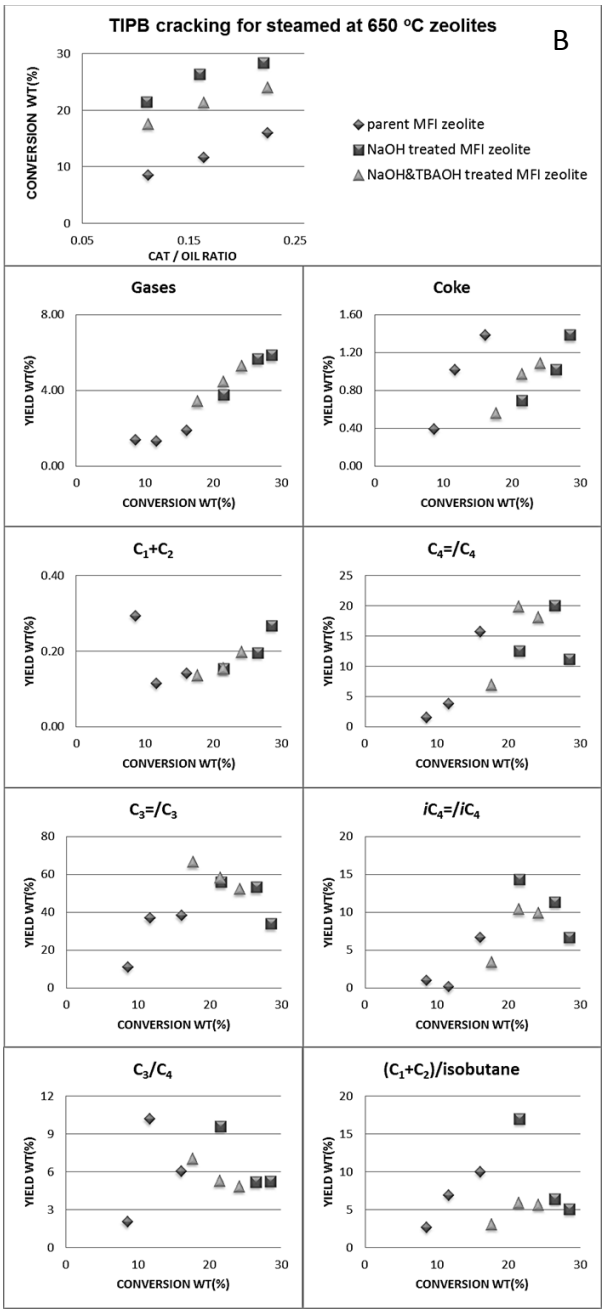
TIPB cracking for steamed at 650 °C zeolites
B
CONVERSION WT(%)
CAT / OIL RATIO
parent MFI zeolite
NaOH treated MFI zeolite
NaOH&TBAOH treated MFI zeolite
Gases
Coke
C_1+C_2
$C_4=/C_4$
$C_3=/C_3$
$iC_4=/iC_4$
C_3/C_4
(C_1+C_2)/isobutane
YIELD WT(%)
CONVERSION WT(%)

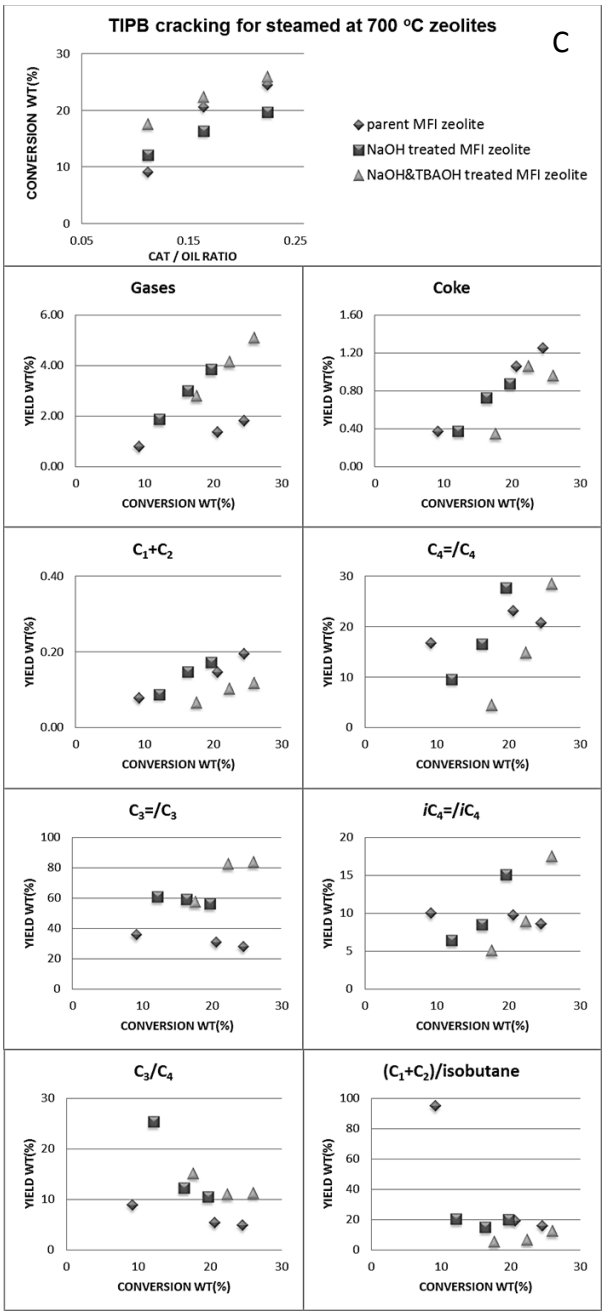
TIPB cracking for steamed at 700 °C zeolites
C
CONVERSION WT(%)
CAT / OIL RATIO
parent MFI zeolite
NaOH treated MFI zeolite
NaOH&TBAOH treated MFI zeolite
Gases
Coke
C_1+C_2
$C_4=/C_4$
$C_3=/C_3$
$iC_4=/iC_4$
C_3/C_4
(C_1+C_2)/isobutane
YIELD WT(%)
CONVERSION WT(%)

Figure 10. Total conversion and selectivities in the cracking of VGO at 520 °C and 30 s time on stream over (a) fresh, (b) steamed at 650 °C and (c) steamed at 700 °C parent and hierarchical zeolites.

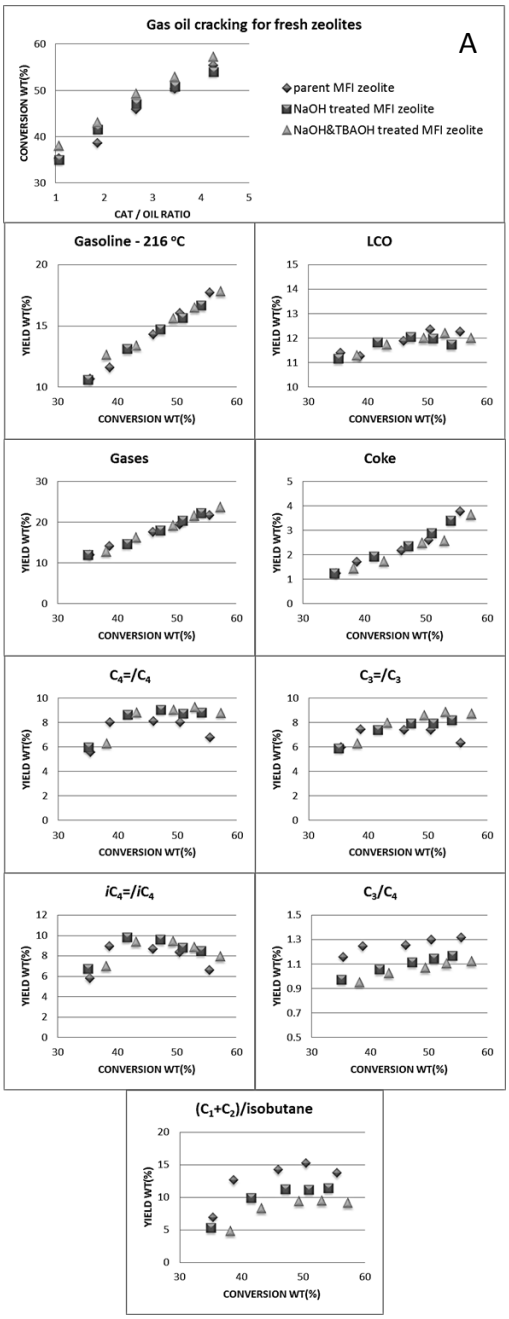

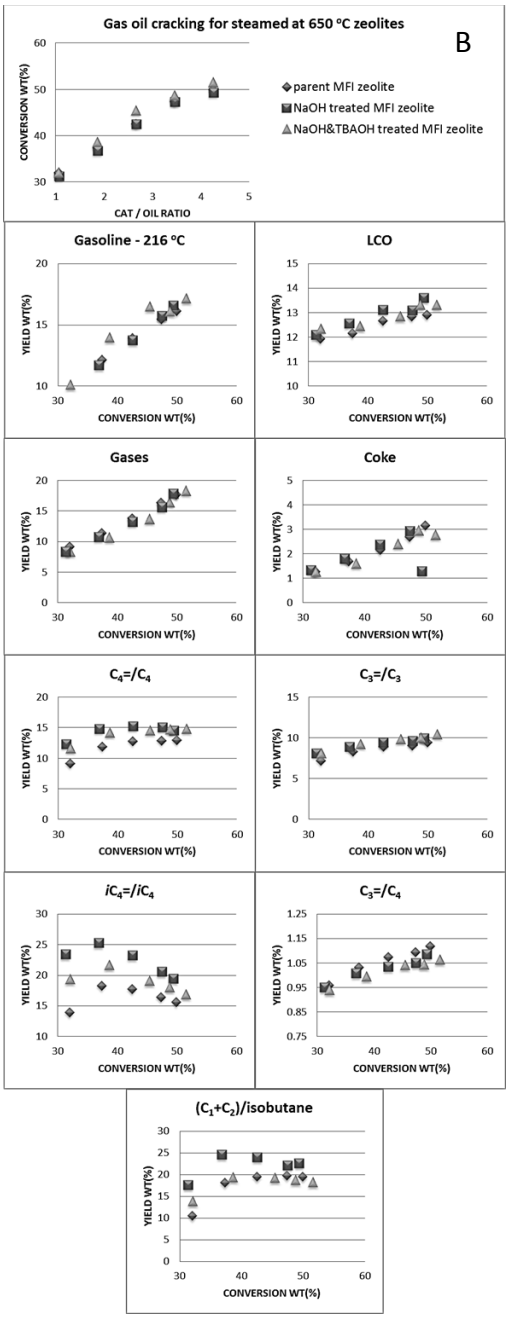
Gas oil cracking for steamed at 650 °C zeolites
B
CONVERSION WT(%)
CAT / OIL RATIO
parent MFI zeolite
NaOH treated MFI zeolite
NaOH&TBAOH treated MFI zeolite
Gasoline - 216 °C
LCO
Gases
Coke
$C_4=/C_4$
$C_3=/C_3$
$iC_4=/iC_4$
$C_3=/C_4$
(C_1+C_2)/isobutane
YIELD WT(%)
CONVERSION WT(%)

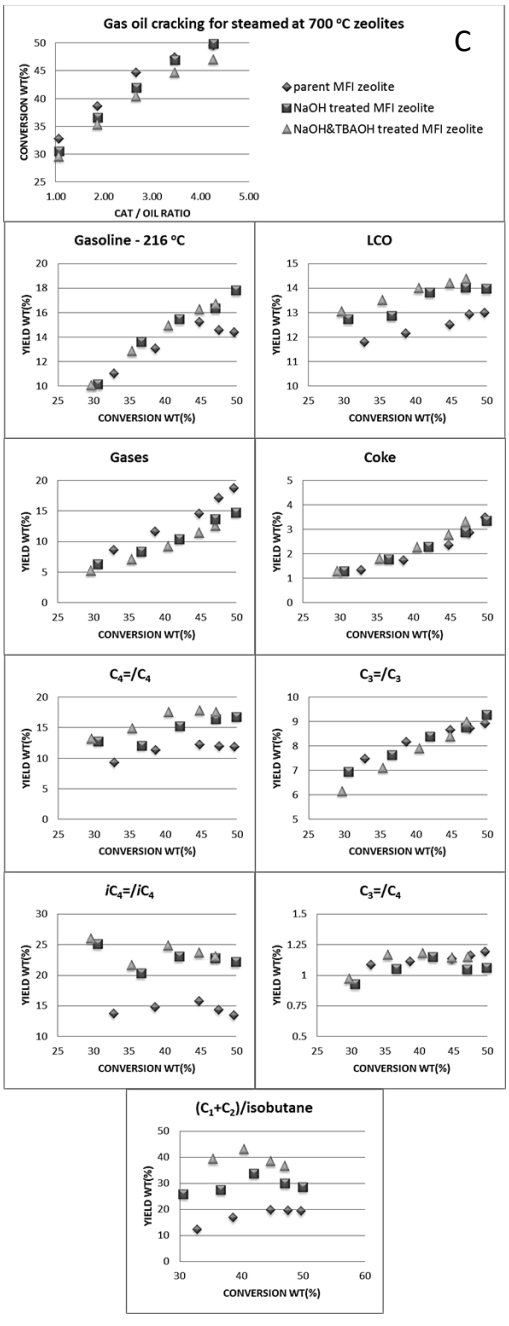
Gas oil cracking for steamed at 700 °C zeolites
C
parent MFI zeolite
NaOH treated MFI zeolite
NaOH&TBAOH treated MFI zeolite
CONVERSION WT(%)
CAT / OIL RATIO
Gasoline - 216 °C
LCO
Gases
Coke
C4=/C4
C3=/C3
iC4=/iC4
C3=/C4
(C1+C2)/isobutane
YIELD WT(%)
CONVERSION WT(%)